DESIGN AND IMPLEMENTATION OF A ROBUST CONTROL SCHEME FOR A SMART JOINT

A Thesis

by

Saher Jabeen

Submitted to the
Graduate School of Sciences and Engineering
In Partial Fulfillment of the Requirements for
the Degree of

Masters of Sciences

in the
Department of Mechanical Engineering

Özyeğin University
January 2017

DESIGN AND IMPLEMENTATION OF A ROBUST CONTROL SCHEME FOR A SMART JOINT

Approved by:

Assistant Professor Özkan Bebek,
Advisor
Department of Mechanical
Engineering
Özyeğin University

Assistant Professor Evren Samur
Department of Mechanical
Engineering
Boğaziçi University

Associate Professor Güney Güven
Yapıcı, Co-Advisor
Department of Mechanical
Engineering
Özyeğin University

Assistant Professor Mehmet İpekoğlu
Department of Mechatronics Systems
Turkish German University

Date Approved: 27 December 2016

Assistant Professor Barkan Uğurlu
Department of Mechanical
Engineering
Özyeğin University

To my beloved parents and husband Talqeeb, who made my dreams

their dreams.

ABSTRACT

The invention of biomedical tools has made medical treatments more convenient; however, manual insertion of these tools requires years of practice and erroneous insertion into the body may cause ruptures and bleeding. Employing medical tools with smart joints can improve the medical procedures making them less traumatic. In this work, a shape memory alloy (SMA) actuator based joint, also known as smart joint, is controlled using a discrete-time integral sliding mode (DISM) control to guide the motion of a smart joint. Two Nitinol based SMA actuators are used in an antagonistic arrangement to provide bending motion.

The controller is designed on the base of a simplified physical model of a single SMA actuator which eliminates the necessity of obtaining an accurate model. A disturbance observer (DOB) is integrated to the controller to compensate the model uncertainties and external disturbances to the system. The bandwidth of SMA actuator is relatively low. Due to the high sampling time of the hardware that is used, a discrete-time controller was designed.

An experimental setup is designed to test the proposed controller with position feedback. In experimental results, DISM controller with DOB is shown to be robust against system model uncertainties and external disturbances. Different frequency responses are compared and it is shown that the response of 0.04 Hz can be achieved with RMS tracking error of 0.0112 radians. Multiple joints connected with rigid links are successfully tracked using electromagnetic Tracking system as the position sensor.

ÖZETÇE

Biomedikal ekipmanlardaki gelişmeler tıbbi uygulamaları daha elverişli bir hale getirmiştir. Ancak bu ekipmanların vücut üzerinde kullanımı uzun süreli pratiğe gerek duymakla birlikte vücuda sokulma sırasında yapılan hatalı uygulamalar yırtık ve kanamalara sebebiyet verebilmektedir. Akıllı eklemlere sahip medikal ekipmanlar kullanılarak, tıbbi müdahaleler iyileştirilebilir ve hastalarda görülen travmalar azaltılabilir. Bu çalışmada, Şekil Hafızalı Alaşım (ŞHA) eyleyiciye sahip eklemin (akıllı eklem), Ayrık Zamanlı İntegral Kayan Kipli Denetim (AZİKKD) ile hareket denetimi sağlanmıştır. Eğme hareketi oluşturmak amacıyla antagonistik düzende bulunan iki Nitinol tabanlı ŞHA eyleyici kullanılmıştır.

Denetleyici, ŞHA eyleyicinin basitleştirilmiş fiziksel modeli üzerine tasarlanmıştır ve hassas bir modele duyulan gereksinimi de ortadan kaldırmıştır. Model belirsizliklerini ve sistem üzerindeki dış kaynaklı bozan-etkenleri karşılamak amacıyla denetleyiciye bir bozan-etken gözlemcisi (BEG) eklenmiştir. ŞHA eyleyicinin bant genişliği görece düşüktür. Kullanılan onanımın düşük örnekleme frekansından dolayı ayrık-zamanlı bir eyleyici tasarlanmıştır.

Önerilen denetleyiciyi test etmek üzere pozisyon geri-beslemeli bir deney düzeneği tasarlanmıştır. Elde edilen sonuçlarda AZİKKD denetleyicisinin BEG ile birlikte sistemdeki belirsizlikler ve dış bozukluları karşı gürbüz olduğu görülmüştür. Farklı frekans cevapları karşılaştırılmış ve 0.04 Hz'lik bir yanıtın 0.0112 radyanlık bir kare ortalama karakök (KOK) takip hatası ile sağlandığı görülmüştür. Esnemez bağlantılar ile birleştirilmiş birden fazla eklem, pozisyon algılayıcısı olarak elektromanyetik takip sistemi kullanılarak başarıyla izlenmiştir.

ACKNOWLEDGEMENTS

TABLE OF CONTENTS

LIST OF TABLES

LIST OF FIGURES

CHAPTER I

INTRODUCTION

In recent years, minimally invasive surgical procedures have found significant importance. Development and advancements of endoscopic technology, instrumentation and video imaging have made it possible to perform the operations without directly touching or visualizing the target structures. Minimally Invasive techniques have largely reduced the risks associated with open surgeries. Potential benefits include less pain and blood loss due to small incisions, low risk of infections, short recovery time, less traumatic, short stay at hospital and less expensive.

In the field of medicine, a breakthrough came with the invention of electric light bulb in 1879 and then a first endoscope with built-in light was introduced by Maximilian Nitze and Josef Leiter. Later on, Johann von Mikulicz and Leiter offered the rigid upper gastrointestinal scope with better cooling system to investigate the esophagus issues safely [1]. Initially, these endoscopes were mainly used for diagnostic purpose such as urology and examination of abdominal cavity.

The minimally invasive techniques are improving with the advancement in the field of visual communication and feedback systems. Visual communication can be considered as back-bone of the modern surgical procedures. In order to perform the surgical procedures physician needs visual information to observe the structure which they need to operate. One such example is endoscope which consists of small camera with a light at the tip of the device. The camera helps the physician to look inside the organs and diagnose the problem without opening any part of the body. Beside diagnostic purposes, minimally invasive techniques are widely used to perform the surgeries of targets which are difficult of access without making large incisions. Some

of the in-practice minimally invasive surgeries includes: Heart [2], Spinal [3], Sinus [4] and different types of abdominal (i.e. laparoscopy) surgeries [5]. [6, 7, 8] presents studies performed to observe the long term effects of using active medical tools for minimally invasive procedures.

Invention of biomedical tools have made medical treatments more convenient; however manual insertion of these tools requires years of practice and erroneous insertion may cause rupture and bleeding [9]. Employing medical tools with smart joints can improve the medical procedures making them less traumatic.

1.1 Shape Memory Alloys

Shape memory alloys (SMAs) are being utilized for specific applications due to their unique characteristics such as recovering large strain values of up to 8% and exerting large forces due to the shape memory effect (SME). SME arises from the ability of the material to possess a specific phase at a specific temperature and be able to transform between phases. SMA actuators work on the principles of thermodynamics. The motion is produced as the SMA changes its physical shape when heated above its transformation temperature. SME effect can be used as two-way or one-way memory. In two-way SME, material changes its shape when heated above the starting transformation temperature value of austenite phase and can return to original value upon decreasing the temperature below martensite transformation temperature value. While, in one-way SME, material deformed at lower temperature can regain its memorized shape provided the temperature higher than austenite phase transformation temperature.

All these unusual aspects have made SMAs potential candidates for various engineering applications [10]. Bio-compatible nature [11] and the super-elastic property [12] made the SMAs special material for medical applications like, artificial muscle [13], stents [14], active catheters [15], needles [16], etc. The property of high power to

weight ratio of SMAs is an additional benefit to use them as an actuator for medical devices which is key point to have the compact design.

1.2   Motion control of a smart joint

To control the maneuverability of a smart joint, a guidance method is needed. SMA actuated joints can be driven by conventional methods of image processing such as using MRI as guidance [17]. Moreover electrical resistance, magnetic properties [18], electromotive power and thermoelectric power of SMAs can be used to control the actuation of the joint. Another common method is to utilize sensor feedback systems to realize the motion of the joint, such as temperature [19] and position sensors. In order to avoid additional sensors, techniques have been introduced to achieve feedback through change in SMA physical properties like change in resistance during phase change [20]. Using the physical properties of SMA as a feedback can be challenging if the disturbances or environmental data is not available. Physical properties of SMA are vulnerable towards environmental changes and that makes them unreliable as a feedback system.

To perform the motion control of SMA actuators, using PID (Proportional-Integral-Derivative) controller is widely found in literature. Due to the fact that environmental changes can cause major changes in the properties of SMA hence changing the model parameters, a simple controller may not perform equally well [21]. In literature, the commonly used technique to enhance the robustness of PID controller is the addition of feed-forward compensator based on the plant model with a feedback system. SMAs possess a nonlinear physical model and model parameters rapidly change with environmental changes of the system. This variability of the system's model parameters can make the controller's job challenging. A PID controller with feed-forward technique can perform well if an approximate model of the actuator is provided. Mostly, researchers put a lot of effort to obtain a precise model of SMA actuator to design a

reliable controller. Jayender et al discussed the importance of obtaining the accurate mathematical model which should represent the actual physical process instead of a mathematical relation obtained by experimental data [22]. In this study, the aim is to reduce the effort required to obtain the model of an SMA actuator, without compromising the performance of the controller.

In medical applications, precise position control is crucial to achieve the target structure without damaging the healthy tissues. To fulfill the need of precise position control, one need to select the most reliable feedback system which must be independent of the actuator performance and environmental effects. A small, light weight sensor is required to attach to the joints to get position feedback.

Next section will provide the brief review of the technologies used in the medical devices for position feedback.

1.3 Overview of tracking technologies

In the modern age, medical procedures have become more convenient with the aid of computer assisted medical devices. The core component of these devices is the guidance system which provides feedback to the operator to perform the relevant action. Depending on the area of operation, guidance method can be selected. Widely used guidance instruments in medical devices includes Ultrasound, Computed tomography(CT) Scan , Magnetic resonance imaging (MRI) and Optical tracker. Some of the methods needs exposure to the target part which is also called as line-of-sight. For the medical applications where the device is inserted in the body through small insertions, cannot have line-of-sight. Similarly, Ultrasound, MRI and CT Scan cannot be reliable or easily implementable for all type of procedures. For such case, most widely used intervention is electromagnetic system which doesn't need line-of-sight and is small enough to be fixed in small medical devices like endoscopes, catheters and needles to perform inside the human body.

Figure 1: Northern Digital Inc. Electromagnetic tracking system used as feedback system for position control of multiple joints. (a) System Control Unit SCU. (b) Sensor Interface Unit SIU. (c) Field Generator FG. (d) 5 DOF sensor. Photo courtesy of Northern Digital Inc.

With all its benefits, electromagnetic system also has some drawbacks. Understanding the limitations of the system is important to guarantee the reliable results as it can cause injuries to the patient.

1.3.1 Electromagnetic Tracking System

To track the motion of the smart joints in real-time, Electromagnetic Tracking System (EMTS) is selected as they are light weight and can fixed inside the joint. A 5 DOF sensor from Northern Digital (NDI) Inc. is utilized to track the orientation of the joints about fixed axis. A sensor interface unit (SIU) collects the sensor data and after some processing send it to system Control Unit (SCU) which calculates position and orientation of the sensor. SCU can provides real time data with up to 40 Hz of refresh rate. A planner field generator fixed at table provides magnetic field. All the components of the tracking system are shown in Fig. 1.

1.3.2 Electromagnetic system error source and accuracy

Source of errors for electromagnetic system can be classified as built-in system error and error due to magnetic field distortion. System error can be reduced by calibration which is usually done by the manufacturer and some random errors can be reduced using filters. One drawback of electromagnetic system is the high sensitivity of magnetic field. Any distortion in magnetic field can cause large error and affects the reliability of the sensor data. It is important the understand the environment in which electromagnetic system's reliability wouldn't be affected. Some sources for distortion can be Ferromagnetic materials, Eddy currents induced by the magnetic field in other conductors or external source of current inside the field [23]. One should avoid any possibility of distortion in magnetic field to obtain accurate results.

Most of the medical procedures includes metal instruments and other electronic devices. It is important to set the environment for the procedure before introducing the electromagnetic system. In our application, main source of distortion was the metallic spring which is used in the design of the joint. Hence, non-ferromagnetic material is used instead.

Thus, in this research commercially available Electromagnetic tracking system is used to get the position feedback. Electromagnetic tracking system is widely used in medical applications as it free the user from line-of-sight limitation and can provide up to 6 DOF motion control.

1.4 Motivation

The aim of this work is to utilize the simplified phenomenological model of a single SMA wire to design the position control of the SMA actuated joint. The sliding mode control (SMC) approach is well known to be an efficient tool to design robust controller for nonlinear systems under uncertain conditions and is well known for the simplicity of its design. Low sensitivity towards plant parameter variations and disturbances is

the major advantage of SMC. This eliminates the necessity of exact modeling. Hence, SMC method is chosen to establish the controller of the SMA joint with a roughly estimated model of the single SMA actuator. A roughly estimated model used to design the controller was further simplified by linearization. A disturbance observer is augmented to compensate the errors due to any external disturbance to the system such as external stresses and mainly due to uncertainties introduced by simplification of the model.

1.5   Thesis Outline

The thesis is organized as follows:

In the current chapter, Chapter 1, brief introduction to shape memory alloys and their actuators was given. Also, the control schemes used in literature for SMA actuators was summarized.

In Chapter 2, modeling of SMA actuators is described in detail. An approximate SMA model is presented by making some assumptions and linearization. Model comparison with experimental results is also given at the end of chapter.

In Chapter 3, a robust control scheme based on Sliding Mode Control in discrete-time is presented to handle the model parameter uncertainties and external disturbances. Controller was tested for position control of single SMA actuator and results have shown satisfactory control performance.

In Chapter 4, results for position control of a single joint are discussed for different scenarios and an encoder with 0.6 resolution was used to get position feedback in terms of bending angle. Bending and resetting actuators were tested in antagonistic motion. Limitations of joints continuous motion are discussed along the solution to the problem. Moreover, position control of multiple joints is presented. Electromagnetic Tracking system is used to get position feedback. Joints are controlled independently and results are shown at the end of the chapter.

CHAPTER II

SMA ACTUATOR: CHARACTERIZATION AND MODELING

This chapter describes the process of transformation of the SMA wires to the actuators along characterization and modeling of SMA actuators. In our application, SMA wires are heat treated to perform bending and resetting action. For bending motion, SMA wires are trained in arc-shape as shown in Fig. 2. Characterization process of arced-shape SMA wire is different than straight shape wire. Ayvali [24] explained the characterization process for arc-shape SMA actuators in detail. To reduce the effort required for characterization and modeling of SMA actuators, a simplified version of SMA model is introduced.

2.1 SMA Actuator and Joint

Most commonly used SMA Actuators are based on nickel-titanium alloy in the shape of a wire. These high strength wires are corrosion resistant and can work for up to 8% of mechanical strain. Nickel-titanium alloy also known as Nitinol is stimulated by law of thermodynamics. Amount of heat required to start and complete the simulation depends on heat treatment. By changing the heat treatment parameters such as time, temperature and cooling method, stimulus properties can be obtained according to the application. In engineering applications, electrical current is a convenient way of generating heat precisely which increase the usability of SMA actuators. Nitinol wire-based SMA actuators are widely used in engineering applications including but not limited to medical devices, automation industry, computer and many industrial products.
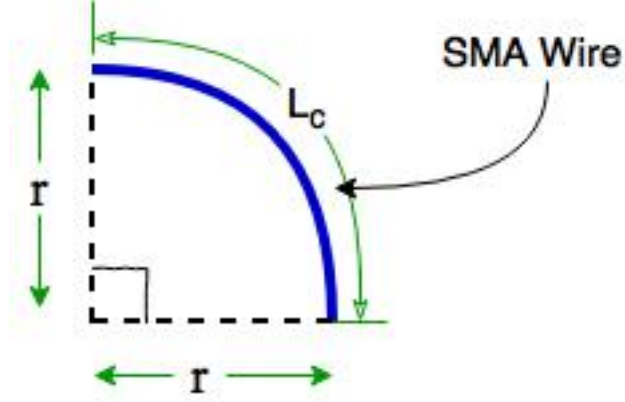
Figure 2: Arc-shaped SMA wire heat treated to perform bending action.

To provide the full actuation to the joint (bending and resetting), commercially available two SMA wires are heat treated. Parameters of heat treatment are selected based on the required properties of the actuators like operating temperature range, stiffness and strength. In medical applications where the device is required to maneuver inside the human body, we are bound to the temperature limits and stiffness.

The smart joint needs back and forth bending motion. For that purpose, two SMA wires are used in an antagonistic way. The bending motion is obtained by treating one SMA wire in an arc-shape and will be recalled as SMA_B. While the other wire is competent of straight shape to perform resetting action and will be recalled as SMA_R. Both wires are heat treated within the limit of 6% of mechanical strain which is recommended to have high life cycle of the actuator [25].

Fig. 3 shows the antagonistic arrangement of the SMA actuators. Solid line represents the bending actuator while dotted line represents the resetting actuator. Bending actuator is heat treated as an arc-shape as shown in Fig. 2 while resetting actuator is heat treated as straight shape. Initially, both actuators are in straight position with temperatures below their respective transition start temperatures which is represented as blue color. While red color shows the temperature of actuators above transition start temperature.
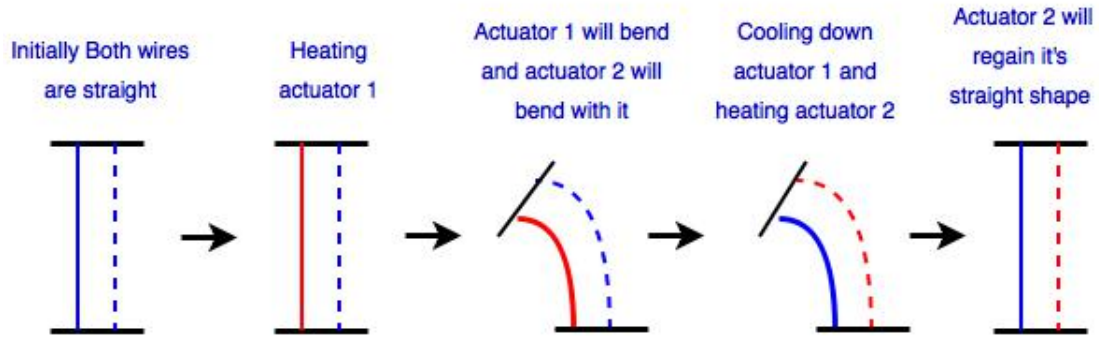
Figure 3: Antagonistic pair of SMA actuators are used to design the bending joint. Actuator 1(Solid line) represents SMA wire with bent memorized shape providing bending action to the joint. While, actuator 2(dotted line) represents the wire with straight shape and is responsible for resetting action.

2.2 SMA Modeling: Literature Review

The most challenging part of using SMA is to have a good understanding of their behavior for the intended application. Till now, several models have been suggested to use SMA in different conditions. We can divide the modeling of SMA into three main parts with respect to the structure of variable used to build a model. They are generally categorized as micro, micro-macro and macro.

In micro approach modeling, micro-scale features are the main subject of interest such as nucleation, twin growth etc [26]. These micro-scale features are good for the basic understanding of SMA material but not really effective to be used in engineering applications. [27] presents micro-macro approach which basically combines the micro-feature technique with macro continuum mechanics in order to get better results. It can be implemented in engineering applications but still not easy to implement as the computational cost for this modeling is really high. Macro or Phenomenological approach deals with macro-level variables to give, not too precise but average behavior of the material which is easy to implement and an efficient way to represent the mechanical behavior of the material.

Phenomenological models can further categorize as models without internal variable and models with internal variables. Examples of without internal variable models are Polynomial potential models [28], [29] and Hysteresis Models [30]. In these models, the behavior of the material is described by stress, strain, temperature and internal energy of SMA. In modeling with internal variable purpose is to describe the change in the internal structure of material with the help of variables involved in phase change, which is the most efficient way to describe the behavior of SMA for engineering applications.

2.2.1 Phenomenological Models of SMA

Various investigations have been conducted to model the SMA for different conditions and applications. The most common modeling technique used in engineering applications is phenomenological model due to its simplicity. Phenomenological models deals with the material's structure properties which can be defined mathematically. The parameters of structure properties can be found through experiments. To obtain the precise model of specific material, all parameters should be find experimentally for each composition of material or different heat treatment. In these models, martensite fraction has been used as an internal variable to describe the shape memory effect as the phase changes. Tanaka , Liang et al and Brinson had done a remarkable work on modeling of 1-D SMAs based on internal variable. Tanaka et al. has presented the basic modeling of 1-D SMAs which then improved and extended by others.

In 1986, Tanaka [31] presented a one dimensional model of the SMA based on internal variable. He explained the shape memory effect based on martensite fraction, strain and change in temperature. The constitutive equation presented by Tanaka explains the stress-strain behavior in terms of change in stress due to change in mechanical strain, temperature and martensite fraction. Variation of martensite fraction during phase transformation was expressed as exponential function as following:

$$\zeta_{M \to A} = exp[\alpha_a(T - A_s) + \beta_a\sigma]$$

$$\zeta_{A \to M} = 1 - exp[\alpha_m(T - M_f) + \beta_m\sigma] \tag{1}$$

where α_a, α_m,β_a and β_m are material constants defined in terms of transformation temperatures, A_s, A_f,M_s and M_f. Moreover, $\zeta_{M \to A}$ represents phase transformation from martensite to austenite and $\zeta_{A \to M}$ represents phase transformation from austenite to martensite which are also called as reverse and forward transformations, respectively.

Liang and Rogers [32] improved the model presented by Tanaka and offered different techniques to model the phase transformation fraction. They used the same concept of constitutive equation but replaced the exponential function to Cosine function in phase transformation model. Moreover, they introduced and proved that external stresses acting over SMA effect the phase transformation process. Also, transformation temperatures change with change in applied stress. The phase transformation model they presented is explained as follows:

$$\zeta_{M \to A} = \frac{\zeta_M}{2}\{cos[a_a(T - A_s) + b_a\sigma] + 1\}$$

$$\zeta_{A \to M} = \frac{1 - \zeta_A}{2}cos[a_m(T - M_f) + b_m\sigma] + \frac{1 + \zeta_A}{2} \tag{2}$$

Brinson et al. offered different technique to model the phase transformation fraction [33] and also filled the gap left by Liang et al. Brinson also compared different models to show that the difference in models is due to employing different kinetics of the phase transformation [34]. Sayyaadi et al [35] presented a comparative analysis of different constitutive models of 1-D SMAs and suggested to use the physical model presented by Brinson to get the precise prediction of shape memory effect. Chung improved the Brinson model further [36].

2.3 SMA Actuator Modeling

Mostly, researchers put a lot of effort to obtain a precise model of SMA actuator to design a reliable controller. Jayender et al discussed the importance of obtaining the accurate mathematical model which should represent the actual physical process instead of a mathematical relation obtained by experimental data [22]. In this study, the aim is to reduce the required effort to obtain the model of SMA actuator, without compromising the performance of the controller. In order to use a simplified model, the model described by Liang [32] is chosen as it represents the physical model of SMA actuator and also fulfilled our requirements.

2.3.1 Continuous Time Model

The physical model of the 1-D SMA presented by Liang et al [32] is utilized to obtain the simplified model. The physical model of the SMA actuator mainly consists of two parts; phase transformation model which gives the relation between temperature and phase change, and the constitutive model which represents the correlation between stress, strain and phase change. Due to hysteresis behavior of SMAs, the phase transformation model for heating (reverse transformation) and cooling (forward transformation) is different. To design a joint, two SMA wires are used in an antagonistic arrangement as explain in section:2.1. Each SMA actuator has only one-way memory with the aim of opposite action which eliminates the need to model the hysteresis. Hence, the reverse transformation(martensite to austenite) is of concern in this case. A brief description of all parts of the single SMA actuator model is given below.

2.3.1.1 Thermodynamic Model

Temperature dynamics of the SMA actuator is based on the thermodynamic model of Joule's heating and with convection heat losses is given in Eq. 3.

$$mc_p\frac{dT}{dt} = I^2R - hA_c(T - T_a) \tag{3}$$

13

where, T is temperature in °C, I is input current, R is resistance, m is mass, c_p is specific heat capacity, T_a is ambient temperature, h is coefficient of convection heat loss and A_c is the surface area of the SMA actuator.
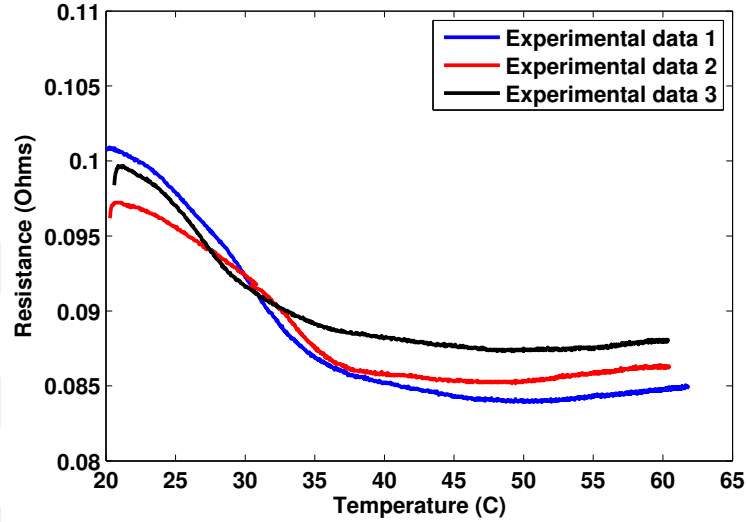
Figure 4: Experimentally found resistance of an SMA actuator.

The resistance of the SMA actuator changes during phase change. Fig. 4 shows the results of experimentally found resistance of the SMA actuator with respect to temperature. It is clearly shown that resistance does change during actuation. To simplify the modeling, resistance is considered as a constant value during actuation. The average value of the data collected experimentally is used in the thermodynamic model.

The other unknown parameter in the model given in Eq. 3 is the coefficient of convection. One may also find it experimentally. The values of specific heat and heat convection coefficient are adjusted by hit and trial method. After adjusting the parameters, temperature model is compared with experimental data. Results in Fig. 5 shows comparison of temperature modeling and experimental data. Three sets of data were collected experimentally by attaching thermocouple directly to the SMA actuator.
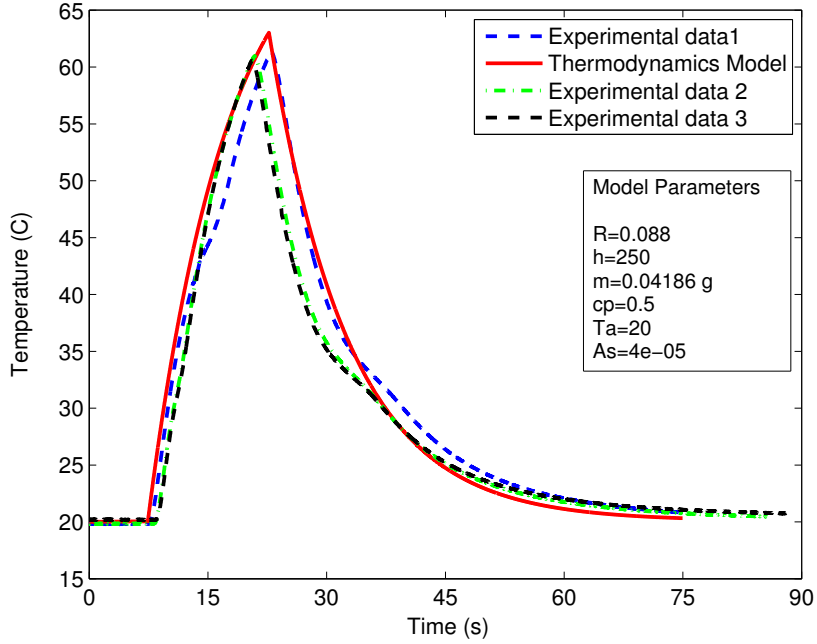
Figure 5: Thermodynamics model established based on Joule's law of heating has shown compatibility with experimental data.

2.3.1.2 Phase Transformation Model

The phase kinetics model gives phase transformation of the SMA actuator based on the actuator's temperature and applied stress over the SMA actuator. Phase transformation model for reverse transformation is given as:

$$\zeta = \frac{\zeta_m}{2}(\cos[a_A(T - A_s) + b_A\sigma] + 1) \tag{4}$$

where, ζ is martensite fraction and its value changes from 1 (martensite) to 0 (austenite) during reverse transformation. ζ_m is the minimum martensite fraction the wire reached during cooling which represents the mix phase state, σ is applied stress, A_s is austenite start temperature, A_f is austenite final temperature, $a_A = \frac{\pi}{(A_f - A_s)}(C^{-1})$ and $b_A = \frac{-a_A}{C_A}$ are constants, and C_A is the stress influence coefficient of the SMA actuator.

15

2.3.1.3   Constitutive Model

SMA's constitutive model shows the correlation between stress, strain and temperature. Stress and martensite volume fraction ζ are the functions of temperature T. The basic equation is given in the form:

$$(\sigma - \sigma_o) = (\varepsilon - \varepsilon_o)E(\zeta) + (T - T_o)\Theta_T + (\zeta - \zeta_o)\Omega(\zeta) \tag{5}$$

where, σ_o is initial stress over the SMA, ε is strain in the wire, ε_o is initial strain, T_o is initial temperature, Θ_T is thermal expansion factor, ζ_o is initial martensite fraction, Ω is phase transformation contribution factor which depends on the maximum recoverable strain, ε_L and is given as $\Omega = -\varepsilon_L E(\zeta)$. E is the modulus of elasticity which vary with phase transformation. For reverse transformation, value of E can be computed as $E(\zeta) = E_A + \zeta(E_M - E_A)$. E_A is the modulus of elasticity in austenite phase and E_M is the modulus of elasticity in martensite phase.

2.3.1.4   Kinematic Model

For our application, desired output is bending angle while constitutive model gives the strain in SMA wire in terms of martensite fraction. To obtain the relation between strain and the bending angle of the SMA wire, simple bending beam theory is assumed which is also described in detail in [37]. According to the beam theory, strain and bending angle relation is given below:

$$\varepsilon_b = \frac{\theta d}{2l_c} \tag{6}$$

where, ε_b represents strain in the SMA wire according to beam theory, d is diameter of wire and l_c is length of curved SMA wire.

2.3.2   Simplification of System Model

The model of SMA actuator presented in section 2.3.1 was simplified by following the assumptions described below. For physical model, assumptions were made by carefully considering the model derivation described in [32].

2.3.2.1   Assumptions

- No convection heat loss, $h = 0$. Eq. 3 simplifies to:

$$\frac{dT}{dt} = \frac{I^2 R}{m c_p} \tag{7}$$

- No external stress applied over SMA, $\sigma = 0$ and SMA exists in pure martensite phase at room temperature, $\zeta_m = \zeta_o$. Phase transformation equation (Eq. 4) simplifies as:

$$\zeta = \frac{\zeta_o}{2}(\cos[a_A(T - A_s)] + 1) \tag{8}$$

- Ignoring strain due to thermal expansion, $\Theta_T = 0$ and assuming no change in applied stress over the SMA wire, $\sigma - \sigma_o = 0$. After inserting value of Ω, constitutive equation (Eq. 5) simplifies as:

$$\varepsilon = \varepsilon_o + (\zeta - \zeta_o)\varepsilon_L \tag{9}$$

Finally, to obtain the output of the SMA model in terms of bending angle, it is required to redefine the strain, ε describe in Eq. 9 to be used as ε_b, in Eq. 6. In terms of phase theory of SMA, residual strain ($\varepsilon = \varepsilon_L$) in martensitic phase can be generated at temperature below martensite start temperature. Residual strain generated in the body then can be recovered completely by heating the SMA above austenite final temperature which makes $\varepsilon = 0$. According to phase transformation, material recovers the martensitic strain, upon heating above austenite final temperature. For our application, SMA wire is heat treated to get the bent shape and in general beam bending theory, SMA wire contains strain when it is in a bent shape. To overcome this, Eq. 9 is rearrange as follows to define ε_b.

$$\varepsilon_b = \varepsilon_o - (\zeta - \zeta_o)\varepsilon_L \tag{10}$$

17

2.4   Experimental setup

An experimental setup was designed to perform all the tests related to characterization, model verification and to test the performance of the controller for the motion control of the joint. In the setup shown in Fig. 6, an encoder with 0.6° of resolution is integrated to provide the position feed-back in terms of bending angle. Setup can be used to test both the single SMA actuator and the smart joint actuated by two SMA actuators. In the setup, one connector can rotate about its fixed axis where the encoder is attached. While, the other connector is consist of pin connection and is free to slide in horizontal direction. The single SMA actuator is basically a wire which can be fixed by its both ends in the setup. Similarly, the joint can be fixed by its both ends in the connectors. National Instruments hardware is used for data acquisition. PCI-6229 DAQ card was used with SCXI-1000 chassis; SCXI-1102 thermocouple and SCXI 1314 voltage measurement modules to acquire temperature and voltage data which was needed for determining the model parameters of SMA actuator. A programmable power supply from AIM & Thurlby Thander Instruments(TTi) (Model: CPX200) was used. The power supply was connected to the PC with RS-232 serial communication protocol. Labview program was built to acquire all the data synchronously and to implement the control scheme. Communication of the programmable power supply to implement the controller in real-time was also done in Labview environment.

2.4.1   Characterization of Bending SMA Actuator

Commercially available SMA wires are heat treated to be utilized as actuators. Heat treatment process was done by fixing the wires in a mold. After fixing the SMA wires, the mold was placed in the oven at $520°C$ for 30 minutes followed by quenching.

The characterization process is done only for bending SMA wire. Heat treated
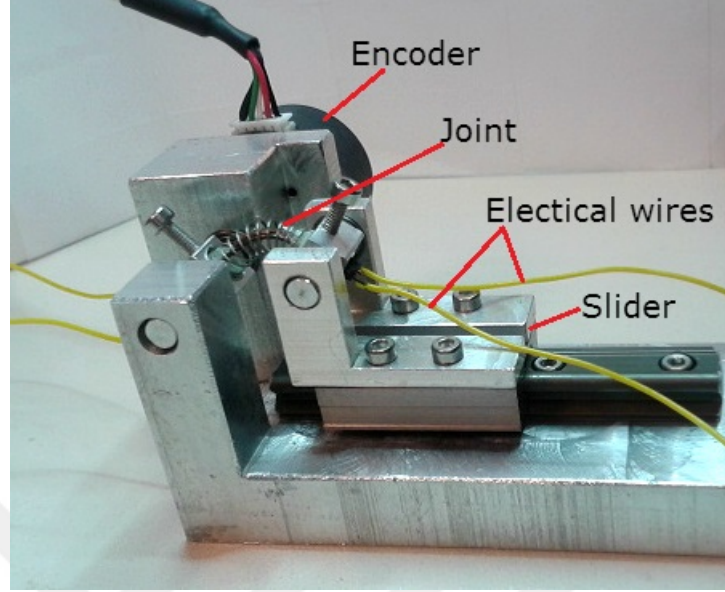
Figure 6: Experimental setup designed for characterization and controller test

SMA wire samples trained for bending motion were tested with Differential Scanning Calorimetry(DSC) device to obtain the phase transformation temperatures. For the reverse transformation, austenite start and final temperatures are obtained as $A_s = 35°C$ and $A_f = 45°C$, respectively. In model simplification, an assumption was made that there is no external stress acting on the system which eliminates σ and b_a from Eq. 4. Hence, it is not required to find C_A value. C_A was required to calculate the material constant b_a ($b_a = \frac{-a_a}{C_A}$). Moreover, the parameters obtained for SMA_B actuator are also used for the modeling of SMA_R actuator. In this way, modeling efforts were further reduced.

Resistance of SMA actuator is obtained experimentally using Ohm's law. Voltage data was obtained using National Instruments hardware while constant current was applied to the actuator. All material properties required for modeling the SMA actuator are given in the Table. 1.

2.5   Model Verification

Based on the assumptions made, simulation of a single SMA actuator is performed. Tested SMA wire is designed to perform the bending action of the joint and its comparison with experimental data is given in Fig. 7. An encoder was utilized to obtain the motion of the SMA actuator in terms of bending angle. Moreover, temperature data was obtained simultaneously by using a thermocouple directly attached to the SMA actuator. The motion of the SMA actuator is represented as a bending angle with temperature change. The model shows rough compatibility with real system. The phase transformation temperature values obtained by DSC test are in agreement with the experimental data of the single bending SMA actuator motion. Model simplification is the main source of error in simulation. Simplification was done to reduce the effort to obtain the model for control design and the process is described in Section. 2.3.2. Moreover, the setup designed for testing also offers some mechanical resistance which is external disturbance in terms of stress over the actuator. This roughly estimated model is further linearized to design the controller for position control of the SMA actuator. The details are given in Chapter 3.
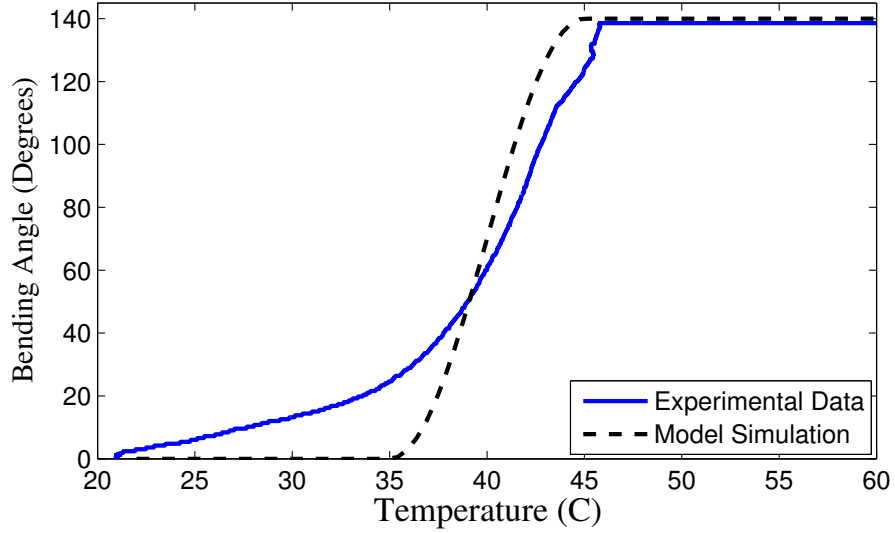
Figure 7: Comparison of experimental data and simulation performed based on simplified SMA model is shown.

Properties of Bending SMA Actuator		
Properties Name	Units	Values
Density, ρ	g/cm^3	6.5
Specific heat, c_p	cal/g-^{o}C	0.2
Diameter, d	mm	0.64
Total length, L	mm	20
Length of curved part, l_c	mm	10
Surface Area, A_c	m^2	4 10^{-3}
Mass, m	g	4.186 10^{-2}
Coefficient of heat convection, h	W/m ^{o}C	250
Resistance, R	Ω	0.9
Ambient temperature, T_a	^{o}C	20
Austenite start temperature, A_s	^{o}C	35
Austenite finish temperature, A_f	^{o}C	65
Max. recoverable strain, ε_L	-	0.0768

Table 1: Properties of bending SMA actuator. Numerical values of h, R, A_s, A_f, ε_L and E are obtained by characterization process.

CHAPTER III

CONTROLLER DESIGN

In control theory, PID (Proportional-Integral-Derivative) controller is widely utilized for linear systems due to its simple architecture. Tuning of PID parameters can be performed either by trial and error method or using the system model. A simple PID controller is linear itself and cannot give satisfactory results for nonlinear systems. Addition of neural and fuzzy logic to the PID controller has improved the performance due to their capability of modeling the nonlinear systems. Carvajal et al. [38] presented the fuzzy logic PID controller capable of handling the known nonlinear system. Chang et al. [39] presented the self-tuning PID controller capable of updating the gain values based on Lyapunov approach. All these approaches can make the controller design complicated.

SMAs posses a nonlinear model and model parameters rapidly change with environmental changes to the system. This variability of system model parameters can make the controller job challenging. A PID controller addition with feed-forward technique can perform well if an approximate model of an actuator is provided. Due to the fact that environmental changes can cause major changes in the properties of SMA hence can change the model parameters, a simple controller may not perform equally well [21]. Addition of self tuning, fuzzy logic, feed-forward technique and/or a disturbance observer to the PID may solve the problem but can make the controller design complicated. This research aimed to design a nonlinear robust controller with simple architecture for a nonlinear system with uncertain parameters and external disturbances.

The sliding mode control (SMC) approach is well known to be an efficient tool

to design a robust controller for nonlinear systems under uncertainty conditions and is well known for the simplicity of its design. Low sensitivity towards plant parameter variations and disturbances is the major advantage of SMC. This eliminates the necessity of the exact modeling. [40], [41], [42] and [43] are few examples of implementation of the SMC for position control of the SMA actuators. Hence, SMC method is chosen to establish the controller of the SMA joint with a roughly estimated model of the single SMA actuator.

In this research, a continuous-time nonlinear model of the SMA actuator has been established. Hence, linearization of system model is required to obtain the linear equations of the system. Section 3.2 will provide the details of the formulation of the system's equations and discretization of the system model to design a discrete-time controller.

3.1 Sliding Mode Control

In continuous-time control systems, the SMC also known as Variable Structure Control (VSS) is renowned for its robustness towards uncertainties of system model parameters. Durability of its robustness arise from its distinct feature of high switching frequency between two states. Basic principle of SMC systems is to drag the states of the system to the desired surface in finite time which is called as sliding surface. After reaching to the desired states, SMC retains the states of the system in close vicinity of the sliding surface. Typical procedure of designing a SMC is consists of two steps: Proposing the sliding function and a control law which can attract the switching surface to the sliding surface. For a continuous-time nonlinear system given as:

$$\dot{x} = g(x, t, v) \ x \in^{n}, \ u \in^{m}$$

$$y = h(x, t)$$

here, x denotes system's states, y is output and v is input to the system. Generally, sliding function is defined in terms error terms and its derivatives. In other words,

purpose is to drive the system states to the surface such that the error become zero in finite time hence, making sliding function reach to zero, $\psi = 0$:

$$\psi = f(e, \dot{e}, ...e^{(i)})$$

where error is defined in terms of output, y and desired output, y_d as:

$$e = y - y_d$$

Second step is defining the control law which is responsible for keeping the system states close to the sliding surface. The most basic linear sliding mode control is a signum function of sliding surface:

$$v = -V sgn(\psi)$$

which is:

$$v = \begin{cases} -V, & \text{for } \psi > 0 \\ \\ V, & \text{for } \psi < 0 \end{cases}$$

where, V is positive gain. Hence, upon reaching steady state the control variable $'v'$ will go back and forth between $v = -V$ and $v = V$ at (theoretically infinitely)high frequency. In real world, systems are dealt in discrete nature and are sampled at limited frequencies mainly due to the processors which are digital. This high switching frequency of SMC system in practice is discontinuous which arises a phenomenon known as Chattering. Chattering is undesirable and sometimes dangerous in practice. [44],[45] and [46] are few examples of studies about chattering free (smooth) SMC for continuous-time systems.

For sampled-data systems, it is of more importance to design a discrete-time controller as the variable switching frequency of SMC is then limited by sampling period, τ. A digital system with long sampling interval may become unstable with continuous-time controller [47]. Our targeted system has low response frequency
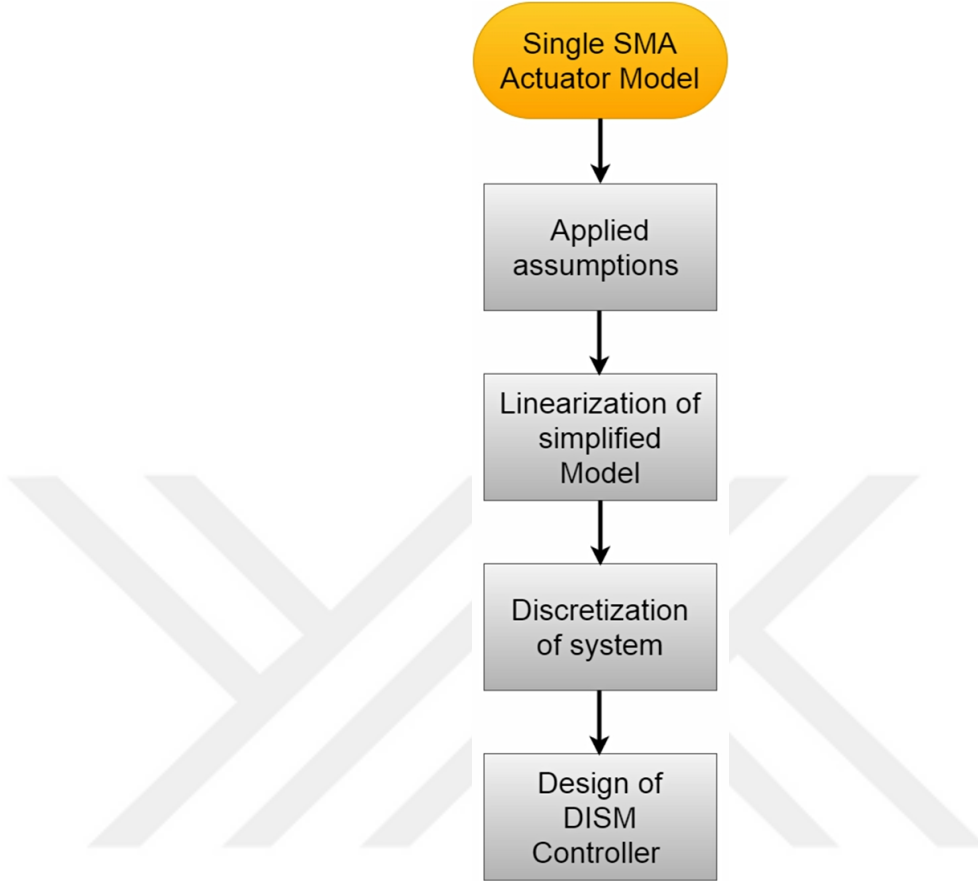
Figure 8: Steps involved in designing the discrete-time control system

hence, a discrete time controller is essential to guarantee the better performance. In recent years, importance of using a discrete-time controller is realized. Another major benefit obtained by discrete-time SMC is that it overcomes the chattering phenomenon [48], [49]. Moreover, stability analysis are done and error boundaries are defined for discrete-time SMC [50], [51], [52].

To start with SMC design, linear input/output equations are required. A basic

Figure 9: Flow diagram showing modeling steps

flow diagram shown in Fig. 8 explains the steps involve in establishing the discrete-time control scheme. In [49], Abidi et al. described the procedure of development of Discrete-time Integral Sliding Mode Control (DISMC) which has properties of continuous-time integral sliding mode control. The procedure includes discretization of continuous-time model of the system and development of the discrete-time controller based on the parameters of the discrete-time model.

3.2   *Linearizaition and Formulation of System Equation*

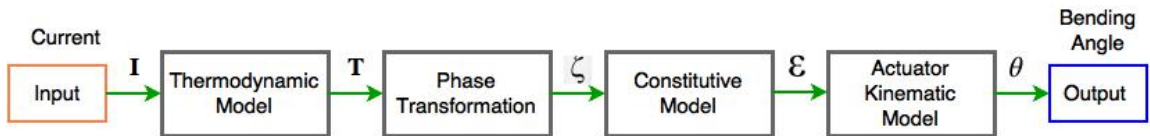Designing of DISMC system requires linear equations of the system in state space. For Single Input Single Output (SISO) targeted system, input and output is current(I) and bending angle(θ), respectively. Nonlinear model of the targeted system described in Chapter. 2 is presented in four parts, Thermodynamics model (Eq. 7), Phase transformation model (Eq. 8), Constitutive model (Eq. 9) and kinematic model (Eq. 10). Fig. 9 shows the connection of all physical models to obtain the output in terms of bending angle.

A nonlinear equation $\theta(T)$ (Eq. 11) is obtained by combining kinematic, constitutive and phase transformation models. The nonlinear equation presenting θ in terms of T is then linearized about average temperature (T_o). T_o is average of austenite start (A_s) and austenite final (A_f) temperature. A_s and A_f are respectively minimum and maximum temperature values during phase transformation, and hence, chosen as a point of linearization. Linearized equation (Eq. 12) is then rearrange as $T(\theta)$ (Eq. 13) followed by differentiation with respect to time. Two differential equations of Temperature (Eq. 14 and Eq. 7) are combined to obtain a single differential equation (Eq. 15). Finally, the linear differential equation is written in state space to develop the discrete-time model of the system. Steps involved in development of continuous-time linear differential equation describe above are given below:

- Combine Eq. 6, 8 and 10 with $\varepsilon_o = 0$ to obtain relation between θ and T:

$$\theta = k - k\cos[a_A(T - A_s)] \tag{11}$$

where, $k = \frac{l_c \varepsilon_L \zeta_o}{d}$ is constant.

- Linearize Eq. 11 about average temperature T_o:

$$\theta(t) = KT(t) + H \tag{12}$$

where, K=$k.\sin[a_A(T_o - A_s)]$ and $H = k - T_o K - k.\cos[a_A(T_o - A_s)]$ are constants.

- Rearrangement of Eq. 12 gives:

$$T(t) = \frac{1}{K}(\theta(t) - H) + d_1 \tag{13}$$

d_1 is the error term introduced by linearization.

- Taking time derivative of temperature and bending angle relation given in Eq. 13 gives:

$$\frac{dT}{dt} = \frac{1}{K}\frac{d\theta}{dt} + d_2 \tag{14}$$

where, d_2 represents the derivative of term d_1.

- Comparing Eq. 7 and Eq. 14 gives final relation between the output,θ and input,I:

$$\frac{d\theta}{dt} = \frac{K}{mc_p}I^2 R + d_3 \tag{15}$$

where, d_3 represents the final error term introduced in the SMA actuator model by the mean of simplification and linearization.

The linearized first-order differential equation presented in Eq. 15 is discretized and the model parameters of discrete-time model are further used to design the controller.

3.3   Discrete-time Model of the System

Problem formulation is done by following the steps described in [49]. Consider a continuous-time system with an estimated linear time-invariant model. Following represents the test system:

$$
\begin{cases}
\dot{x}(t) = Ax(t) + Bu(t) + d(t) \\
y(t) = Cx(t)
\end{cases}
\tag{16}
$$

where $x(t)$ represents the state, $y(t)$ output, $u(t)$ control input and $d(t)$ represents the disturbance to the system. The disturbance is considered as an unknown function. A is the state matrix, B is the control matrix and C is the output matrix. Presented system can be written in discrete-time domain as follows:

$$
\begin{cases}
x_{k+1} = \Phi x_k + \Gamma u_k + d_k \\
y_k = Cx_k
\end{cases}
\tag{17}
$$

where the discretization parameters are defined as:

$$
\Phi = e^{A\tau}, \Gamma = \int e^{A\tau} dt B
$$

τ is the sampling period and d_k represents the disturbance caused by accumulation from $k\tau$ to $(k+1)\tau$. From the definition Γ can be represented as:

$$
\Gamma = B\tau + \frac{1}{2!}AB\tau^2 + O(\tau^3)
\tag{18}
$$

By comparing the system defined in Eq. 15 with the discrete-time system established in Eq. 17, parameters of test system in discrete-time domain are obtained as given below:

$$
A = 0 , \quad B = \frac{KR}{mc_p} , \quad C = 1
$$

Sampling time was $\tau = 50ms$ and other parameters of the discretized system were found as:

$$\Phi = 1 \ , \quad \Gamma = B\tau \ , \quad C = 1$$

3.4   Discrete-Time Integral Sliding Mode Control

Basic concept of sliding mode control is to force the system to slide over a desired surface without going into the complexity of the system. SMC is well known for its robustness towards uncertainties of system model parameters but suffers from an undesirable chattering phenomenon. This chattering phenomenon can make the sampled-data system unstable around its steady state. A Discrete-time control scheme has potential to overcome the chattering. The Discrete-time Integral Sliding Mode Control (DISMC) scheme introduced in [49] has characteristics of continuous-time integral function and can perform precise tracking with up to $\bigcirc(T^2)$ steady-state error. The stability analysis and error boundaries for real time systems are discussed in [53].

3.4.1   Output-Tracking ISM Control: State Feedback Approach

In Output-Tracking ISM Control scheme, the sliding function is designed for the purpose of minimizing the tracking error, e (e=output-reference) while state feedback is utilized to design the control law. Here, we are considering the sliding surface as an integral function. The discrete-time design of sliding function is given below:

$$\eta_k = e_k - e_0 + \varepsilon_k \tag{19}$$

$$\varepsilon_k = \varepsilon_{k-1} + Ge_{k-1}$$

where, $e_k = r_k - y_k$ is the tracking error, η_k is sliding function, ε_k is integral component and G is an integral gain. e_0 and ε_0 are initial error and error integral and are set as zero.

The main objective is to drive the state towards and stay on the switching surface

$\eta_{k+1} = 0$ at every sampling instant. The sliding surface (Eq. 19) can be modified as:

$$\eta_{k+1} = e_{k+1} - e_0 + \varepsilon_k + Ge_k$$

Eq. 19, $-e_0 + \varepsilon_k = \eta_k - e_k$ will give the sliding surface as:

$$\eta_{k+1} = e_{k+1} + \eta_k - (I - G)e_k \tag{20}$$

Putting $e_{k+1} = r_{k+1} - C[\Phi x_k + \Gamma u_k + d_k]$ in Eq. 20 gives:

$$\eta_{k+1} = \lambda_k - C\Gamma u_k - Cd_k \tag{21}$$

Where, $\lambda_k = r_{k+1} - (I - G)e_k - C\Phi x_k + \eta_k$ and d_k is disturbance to the system.

By setting $\eta_{k+1} = 0$, the control law can be obtained:

$$u_k{}^{eq} = (\lambda_k - Cd_k)(C\Gamma)^{-1} \tag{22}$$

The final control law with estimated disturbance can be written as:

$$u_k = (C\Gamma)^{-1}(\lambda_k - C\hat{d}_k) \tag{23}$$

3.4.2 Disturbance Observer

The control law defined in Eq. 23 requires the complete knowledge of disturbances. Disturbances to the system are unknown and cannot be modeled hence, the estimation is done. A disturbance observer (DOB) is designed on the base of estimated disturbance from the previous state of the system and control signal. Estimated disturbance is given as:

$$\hat{d}_k = d_{k-1} = x_k - \Phi x_{k-1} - \Gamma u_{k-1}$$

3.5 Position Control of a Single SMA Actuator

First, performance of the controller was tested for model uncertainties. The main source of uncertainties was simplification of SMA actuator's model. A single SMA_B
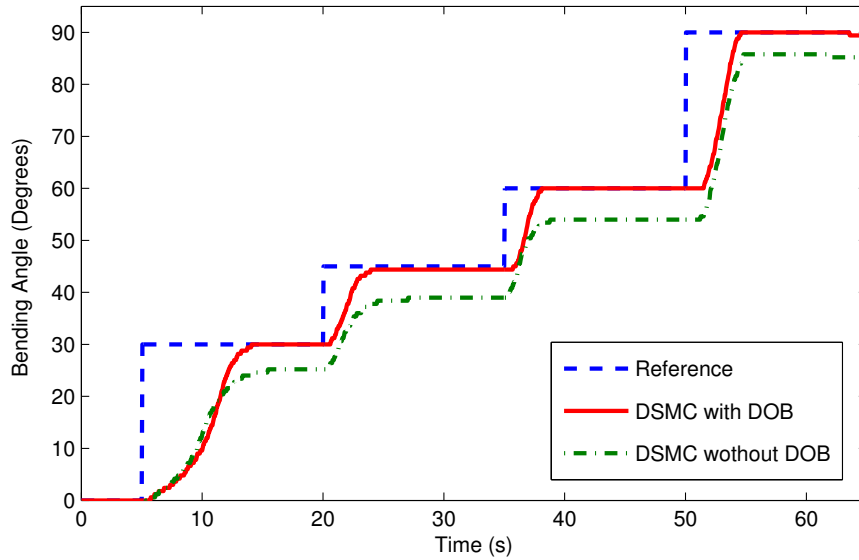
Figure 10: Discrete-time Integral Sliding Mode Control is tested over the single bending SMA wire to observe the effectiveness of the integrated DOB for system parameter uncertainties and external disturbances.

actuator was used to perform the initial tests. Experiment was performed in open environment at room temperature which adds heat loss by natural convection. Moreover, setup offers mechanical resistance which is not modeled. Heat loss, stress due to mechanical resistance and other assumptions made in simplification of the model are the main sources of model uncertainties. These uncertainties are treated as a disturbance to the system and are estimated based on the states of the system. To test the controller tracking performance, a step incremental stair path was given as a reference input and the results are shown in Fig. 10. With integrated DOB, controller tracked the reference precisely. Effectiveness of the DOB was tested by removing the DOB from the controller design as SMC and DOB works independently. It is clearly shown that, without DOB steady-state error is introduced in tracking. This error is due to uncertainties of the model parameters and are well compensated with DOB.

CHAPTER IV

POSITION CONTROL OF SMART JOINT

4.1   Overview

In this chapter, position control of the joint is discussed. Discrete-time sliding mode control designed based on a physical model of SMA_B actuator is implemented over both SMA_B and SMA_R actuators to control the motion of the joint. Before testing the performance of the controller for tracking the continuous motion of the joint, it is tested for position control of the individual actuators. SMA_B and SMA_R actuators are incorporated in a joint in an antagonistic way. In this way, the robustness of the controller was tested for system parameters uncertainties and external disturbance. After successfully testing the controller performance for individual actuators, it was then evaluated for continuous motion of the joint.

During continuous motion test, a problem raised due to insufficient cooling which led to joint failure. In most of the applications, antagonistic arrangement of the SMA actuators is used for the purpose of active resetting to reduce the delays required for cooling in a periodic motion. In this way, working frequency of the actuators can also be improved. The actuators show a reduction in performance if not provided with sufficient time for cooling. To solve this issue, temperature based control is added to the current position control scheme. Position control is based solely on position feedback, no feedback is available for the change in temperature of the actuators. Hence, temperature model based on Joule's heating is utilized to estimate the temperature of both actuators during actuation. A brief description of the joint and control strategy is given in the later sections along with the control test results.
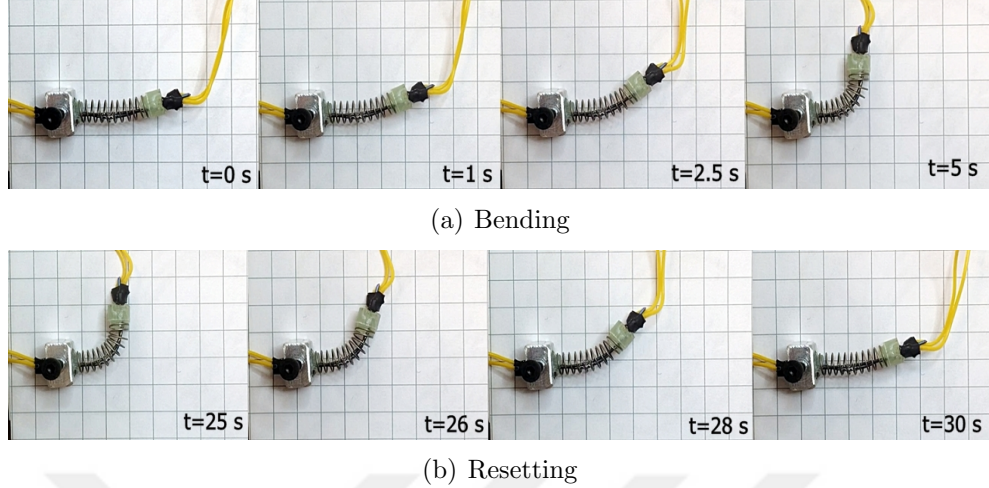
(a) Bending

(b) Resetting

Figure 11: Joint actuation is shown outside the setup. Ideally, joint can actuate at maximum 0.1Hz. Time period of the joint actuation can be defined as 10 seconds without any cooling delay.

4.2 Joint Description

Two commercially available SMA wires are used in an antagonistic arrangement to provide the cyclic actuation to the joint (bending and resetting). For bending motion, an SMA wire is trained for bending motion under 6% of the strain limit while the other SMA wire has a memory of straight shape to perform a resetting action. Fig. 3 shows the antagonistic action of SMA actuators which provides bending and resetting action to the joint. A metallic spring is used as a base structure of the joint. In Fig. 11, full actuation of the joint is shown. First, SMA_B actuator was activated for 5 seconds. After 20 seconds of delay, joint was reset to straight position by activating the SMA_R actuator.

4.3 Controller Performance Test for Position Control of an Individual Actuator

Before performing the continuous motion test of the joint, both actuators are tested individually. As both actuators have different material properties, it is important to test the robustness of the controller for both actuators as integrated parts of the joint to act as bending and resetting actuators. The stiffness of each actuator will
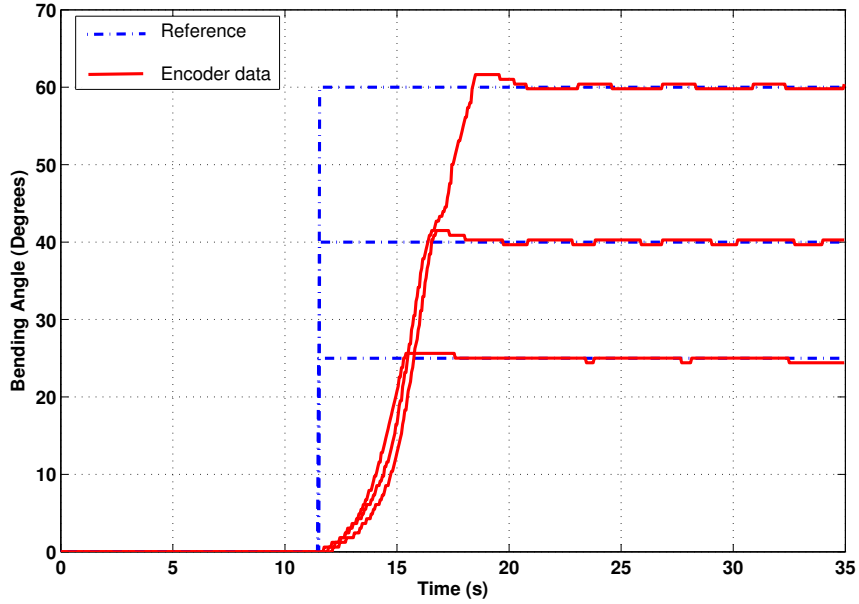
33

Figure 12: Performance of Discrete-time Integral Sliding Mode Control is tested for SMA_B actuator integrated in a joint.

act as an external disturbance while the other actuator is in action. SMAs exert high forces at high temperature and these forces are not estimated. Hence, if the inactive actuator is at a temperature higher than austenite start temperature it exerts force on the active actuator. These forces are not estimated and considered as external disturbances. But the forces should be under the critical stress limit of the actuator as also described in [34]. Otherwise, it will be a physical limitation of the joints actuation and controller cannot perform with the same level of expectation.

4.3.1 SMA_B Actuator

The position control of an SMA_B actuator is tested as a part of the joint. The actuator was tested for different bending levels. Tracking with average steady state error of ± 0.0069 radians for all reference angles is obtained as shown in Fig. 12. Stress due to spring, stiffness of SMA_R actuator and setup motion resistance were acting as external disturbances to the SMA_B actuator during motion.
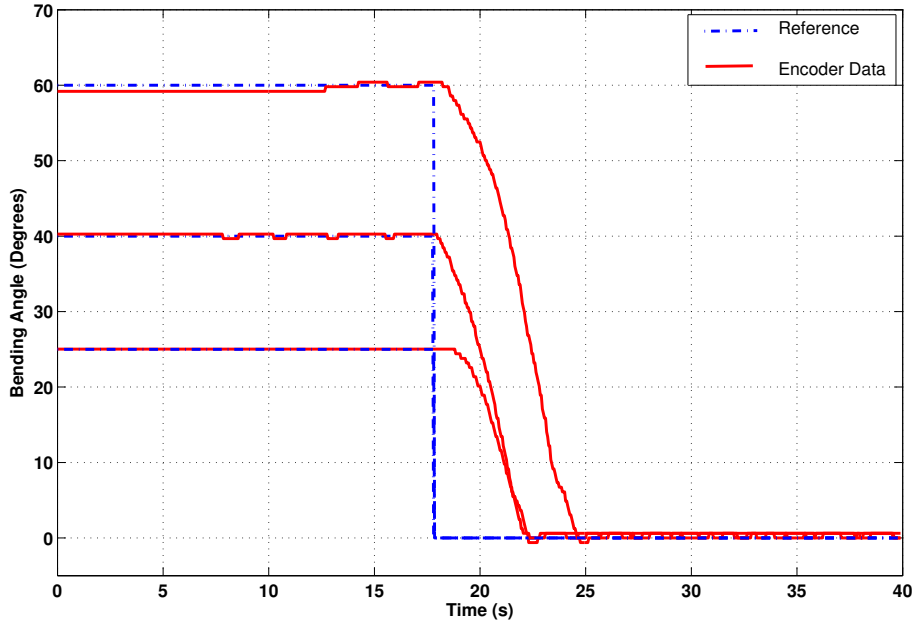
34

Figure 13: Performance of Discrete-time Integral Sliding Mode Control is tested for position control of the SMA_R actuator.

4.3.2 SMA_R Actuator

The position control SMA_R actuator was also tested in a similar manner described for SMA_B actuator. This time target was set to reach back to straight position of the joint while the initial positions were set at different levels of bending angles. Results in Fig. 13 shows the tracking with average steady state error of ± 0.0095 radians. In the case of SMA_R actuator it is required to recall that the controller was designed on the base of SMA_B actuator model. Hence, the model parameter uncertainties were higher which were also well compensated along with external disturbance provided by SMA_B actuator during resetting action. As a result, the robustness of the controller is proven for the system model parameter uncertainties as the controller was designed based on the physical model of an SMA_B actuator. Effectiveness of integrated DOB in the controller design is also observed.

4.4 Controller Performance Test for Position Control of the Joint

After obtaining the satisfactory results for position control of the individual actuators, next step was to test the controller performance for continuous motion tracking of the joint. During the testing of an individual actuator motion, initially both actuators were always at room temperature. Purpose was to make sure that the actuators were not under stress higher than their critical stress values. While during actuation, the heat was transferred from active actuator to the inactive actuator resulting in opposing force over the active actuator. If the force is under the critical stress limit it can be compensated by integrated DOB in the controller design. Heat transfer between two actuators during actuation is shown in the Fig. 14 and the effect of heat transfer over the performance of the joint will be discussed in detail later.

4.4.1 Control strategy

Control strategy for motion control of the joint is described in the block diagram shown in Fig. 15. Depending on the error, the controller generates positive or negative output. A positive value means SMA_B actuator should be activated. Similarly, negative controller output calls for activation of the SMA_R actuator. Both wires are controlled independently with different power sources. Moreover, output of the controller is saturated to avoid overheating in case of any obstacle. Saturation value is selected based on the maximum current amount which can be given to the actuators. Current required to complete the actuation is defined by austenite finish temperature.

4.4.2 Controller Test Results

Basic test was performed by selecting incremental and decremental step input as the reference trajectory. For small steps, the target was achieved with small oscillations of $\pm 0.5°$ of magnitude and can be neglected. The tracking results are shown in Fig. 16 and the tracking rms error was 0.087 radians.
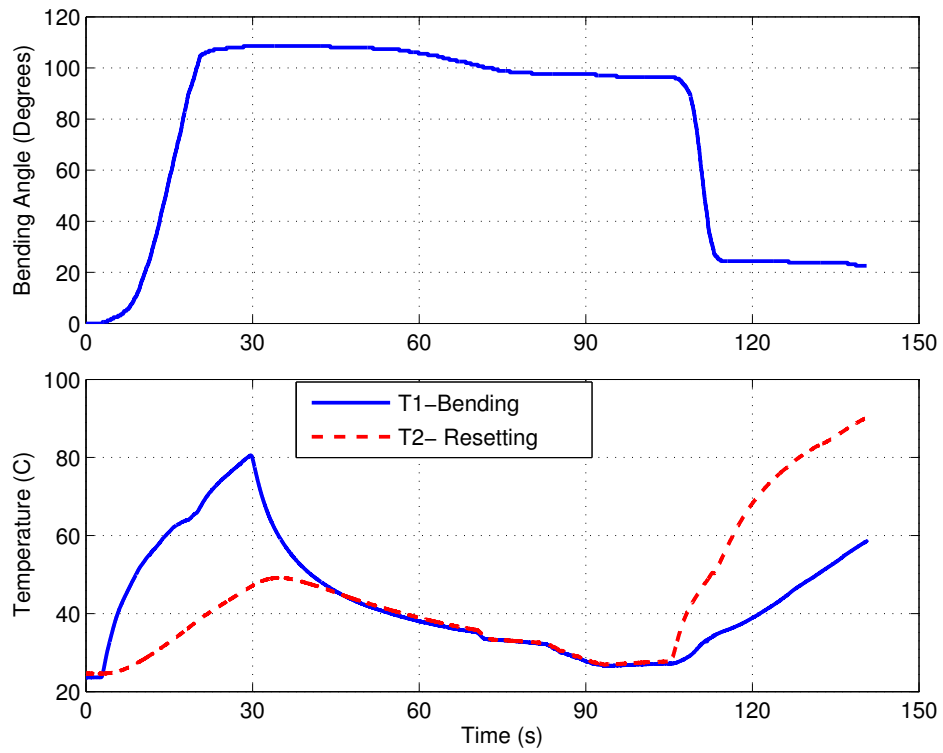
Figure 14: T1-Bending and T2-Resetting represents thermocouple data recoded for bending and resetting actuator during actuation, respectively.
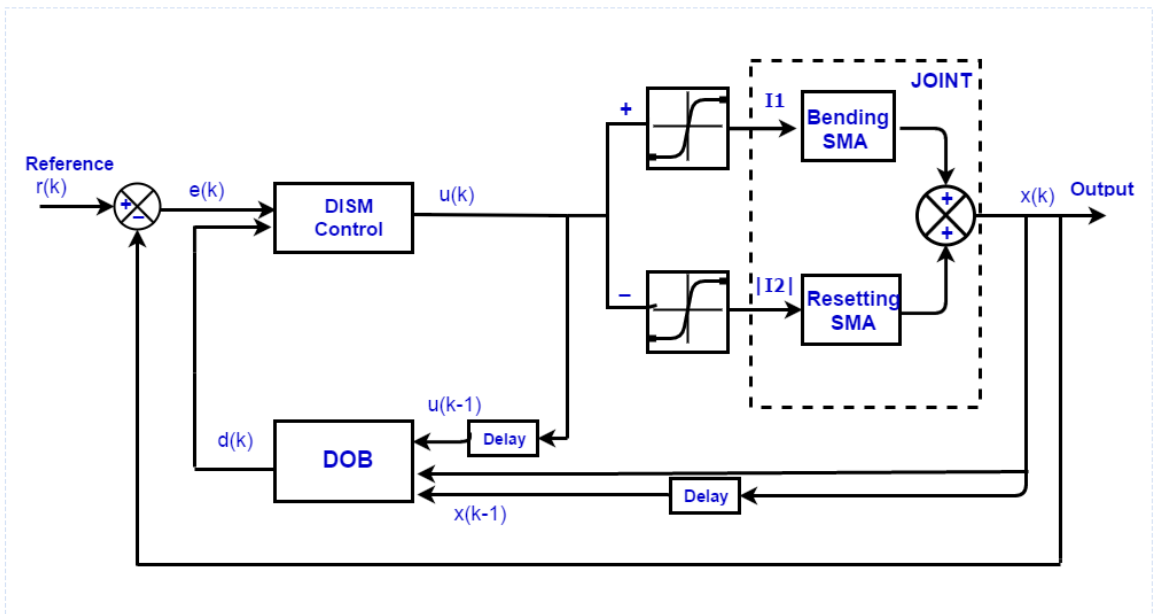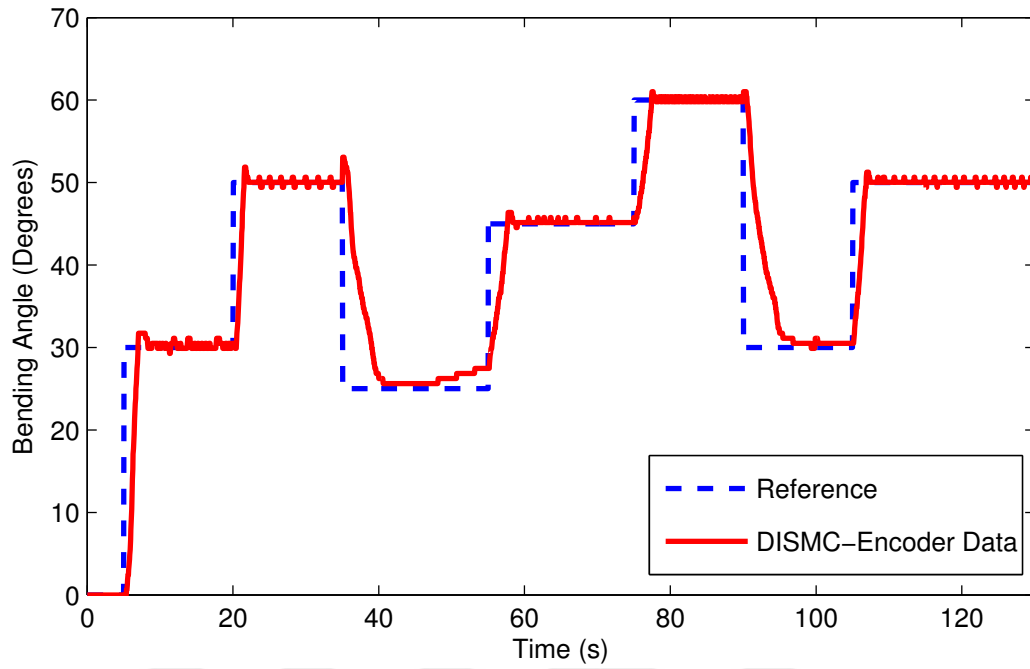

Figure 15: Control strategy for a smart joint

Figure 16: DISMC is tested for position control of the joint in continuous motion with step reference
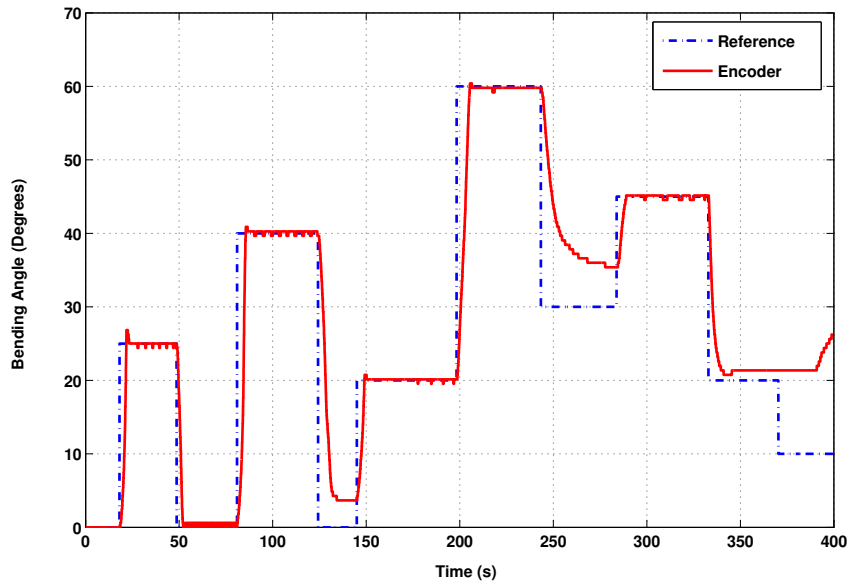

Figure 17: Continuous action of a joint for large reference steps.
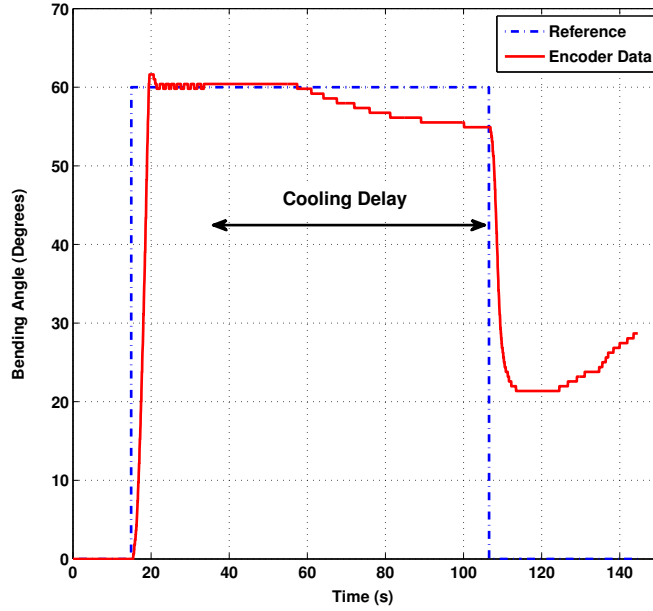
38

Figure 18: SMA$_R$ actuator lost its performance after continuous motion test.

Another set of test was performed for relatively big step size and results are shown in Fig. 17. In the first cycle for 0 to 20 and 20 to 0, joint tracking was achieved with minimum error. In the continuation of the same test, the joint was tracked to the bending angle of 40 degrees and was commanded to go back to the initial position of 0 degrees. But it failed and reached to approximately 10 degrees. In the continuation, bending was achieved successfully for 20 degrees and then for 60 degrees. In further action, joint failed to even reach 30 degrees of resetting angle while joint was initially at 60 degrees of bending position. Eventually, joint failed to perform resetting from 20 degrees to 10 degrees.

To check whether the joint failed or the controller, we tested the joint's actuation by providing enough cooling time between the activation of two actuators to make sure not to have stresses higher than critical stress values. Joint's performance test is shown in Fig. 18 and it is clear that SMA$_R$ actuator lost its performance permanently which also implies that the actuator lost its memorized shape. Temporary loss

of performance happens when the inactive actuator is at high temperature and exerts stresses higher than the critical stress value of the active actuator. While overheating of the actuator at stress higher than it's critical value can damage the actuator permanently.

Second set of tests were performed to check tracking of the continuous sine wave as a reference angle. As we already suspected that continuous motion may not be successfully achieved without active cooling. Hence, different frequency sine wave was tested to check the possibilities of obtaining fastest action. Sine input with 0.028Hz, 0.03, 0.04, 0.05, 0.06, 0.07 and 0.08 Hz was tested as reference signal. Tracking results for selected frequencies are shown in Fig. 19. Total time required for bending and resetting action without any cooling delay was observed as 10 s (0.1 Hz) from the test results shown in Fig. 11. But at 0.08 Hz, the joint couldn't track the sine input as it is shown in Fig. 19(c). On the other hand, the performance of the joint is clearly better at lower frequencies. RMS values of tracking error for all the tested frequencies are shown in Fig. 20.

With natural convection cooling effect, continuous motion tracking with a minimum RMS error of 0.0112 radians can be achieved with 0.04 Hz of response frequency. Error is calculated as difference between the reference and tracked positions. We suspect that an increase in RMS error at lower frequencies was due to heat transfer between SMA actuators and is also shown in Fig. 14.

These results led us to add the temperature threshold control in the current control scheme which is solely based on the position feedback. Details of temperature control are given in the next section.

Next section discusses the overheating problem and high-temperature forces. We will discuss the heating phenomenon in detail with the solution of the problem. At the end, better results for continuous motion tracking are shown with the addition of temperature threshold to the position control of the joint.
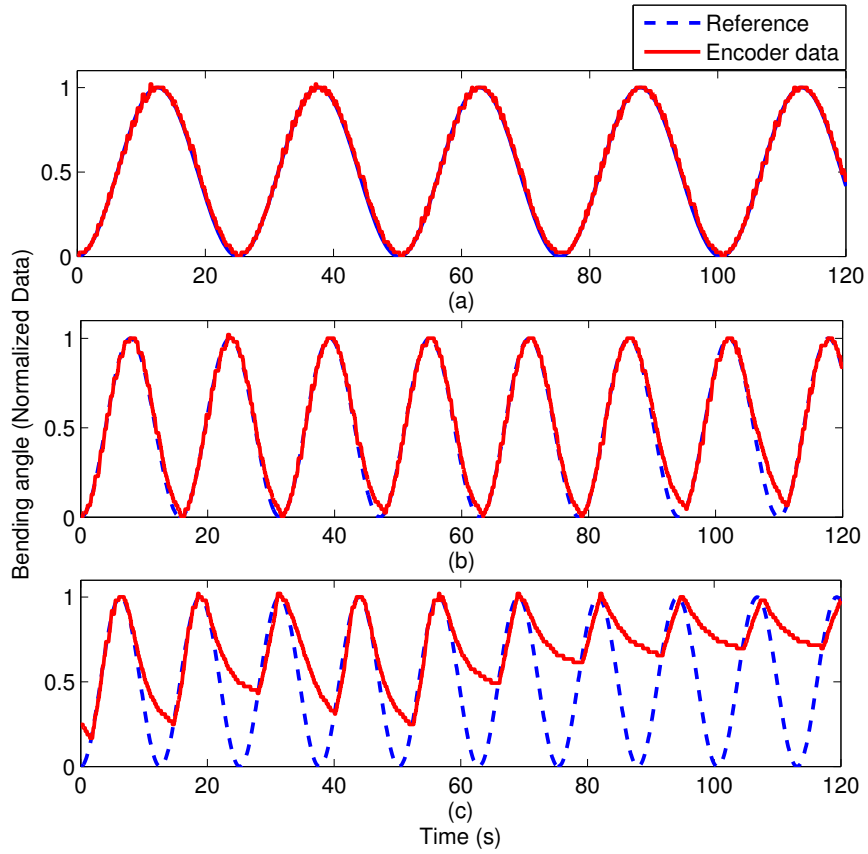
40

Figure 19: Reference signal frequency: (a) 0.04 Hz (b) 0.06 Hz and (c) 0.08 Hz.
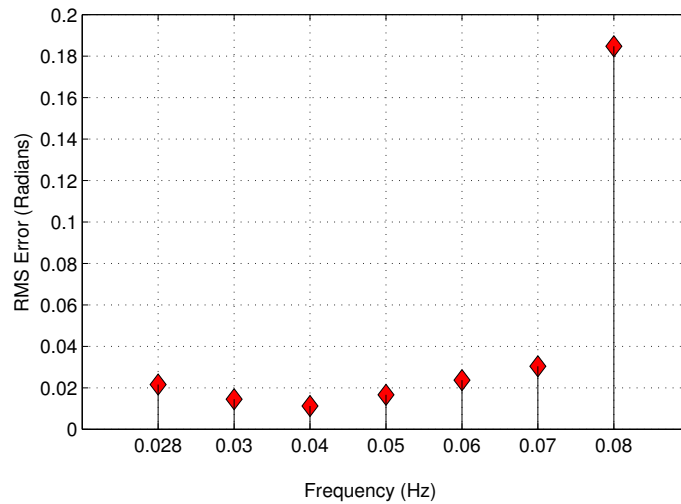

Figure 20: Comparison of tracking error of the tested frequency responses. Minimum tracking error can be obtained with 0.04 Hz of input frequency.

4.5   Physical limitation of Joint's motion

The basic working principle of the Ni-Ti based SMA actuators is thermal energy. Change in temperature cause phase change. For one way memory SMA, the phase change phenomenon occurs when the temperature of the SMA increases than austenite start temperature, A_s and recovers the memorized shape completely when the temperature reaches to the austenite final temperature, A_f. Austenite start and final temperature change with applied stress and can be defined in terms of stress influence coefficient, C_A. The phase transformation temperatures increase with increase in stress. The stress can mainly caused by the force exerted by the other actuator at higher temperature or any other source of resistance to the motion of the actuator.
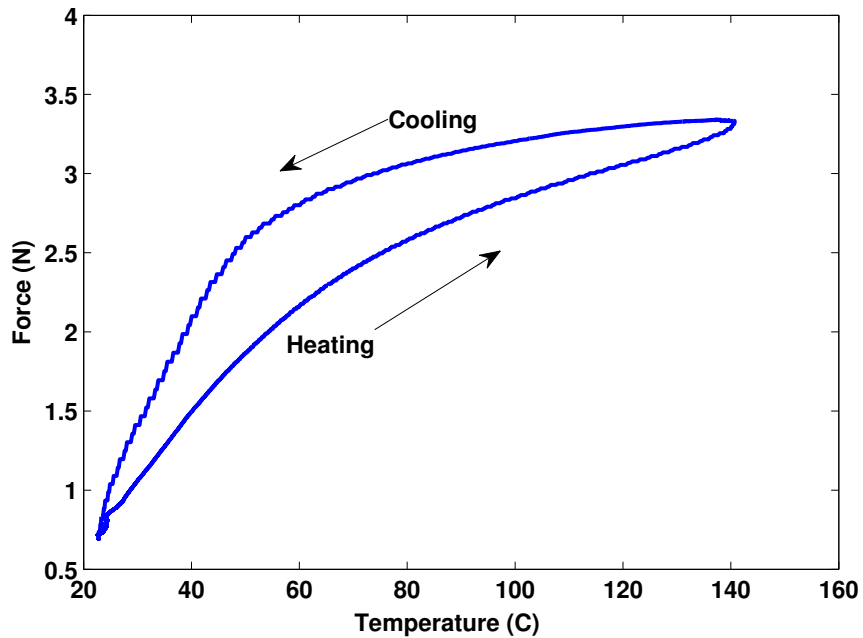

Figure 21: Experimental data collected shows the behavior of the force exerted by the SMA actuator when the temperature changes.

In case, the applied stress over the SMA actuator is higher than the critical stress value, complete phase transformation may not occur completely. The source of stress can be a hurdle in the motion of the joint or by the other wire at high temperature.

Moreover, SMAs exert high forces at high temperature which is critical when two actuators are working in antagonistic way. One can effect the performance of the other if at high temperature. By keeping all the facts in mind, we realized the need of adding temperature threshold limits in the controller as an activation condition of an individual actuator.

While working under stress, it is important to observe the temperature of an SMA actuator during actuation. To understand the problem let's consider the scenario where applied stress is greater than the maximum critical stress. If the applied stress is more than the maximum limit of critical stress then SMA may not be able to recover it's memory completely which in result cause unsuccessful actuation. Meanwhile, controller will put its all efforts to perform the desired actuation. In case of continuous input current, controller can overheat the SMA actuator. Overheating under stress results in failure of the SMA actuator. The actuation of SMA under high stresses is observed during experimentation and was discussed in Section 4.4. In results shown in Fig. 18, reduction in cyclic life of SMA actuator was observed.

In our application, there can be two major possibilities for the SMA to be under stresses higher than critical stress value. One possibility is an obstacle which can block the motion of the joint. In such case, controller can overheat the SMA actuator as there is no force feed-back to estimate the external stress applied over the SMA actuator.

Second major factor which contributes in over stressing the SMA actuator is the force applied by the other actuator. To understand this phenomenon, we should mention that two SMA actuators arranged in an antagonistic way. Each actuator is designed to perform the action against each other to produce cyclic motion. Also, we should revise the behaviour of SMAs at high temperature. At high temperature (during phase change from martensite to austenite), SMAs exerts high forces. Due to the high forces produced by the inactive actuator (which can be at temperature

43

higher than it's austenite start temperature), there is a possibility that the active actuator may experience the stress higher than the critical stress value.

To explain it better, the temperature data of both actuators during actuation is collected. To obtain the bending actuation of the joint, temperature of SMA_B actuator should reach to austenite final temperature. At this temperature, SMA_B actuator exerts force over SMA_R actuator. During the continuation of the joint motion, if we activate the SMA_R actuator to reset the joint right after deactivating the SMA_B actuator while SMA_B actuator would be still at higher temperature. We observed that SMA_R actuator couldn't complete its action and joint failed to reset to zero bending angle. On the other hand, if we wait for the SMA_B actuator to cool down to room temperature before activating SMA_R actuator we observed the successful performance of the SMA_R actuator and joint could reset to the straight position. Reason behind failure of SMA_R actuator in case of first scenario was the fact that stress applied by SMA_B actuator was higher than the critical stress value of SMA_R actuator.

To solve these two issues the temperature threshold is required in the current control scheme which is solely based on position feedback. Basic control strategy is presented in the block diagram shown in Fig. 22.

Implementation of the temperature threshold needs temperature data of both wires during actuation. To obtain the temperature feedback, let us discuss the available options. Possible options for temperature feed-back includes:

- Temperature measurement sensors like thermocouples and RTDs. This will increase the complexity of the system with an additional sensor.

- Measuring temperature of SMA actuators based on change in resistance which includes resistance feed-back. Resistance of the SMAs change with temperature. The temperature of an SMA can be modeled in terms of its resistance.
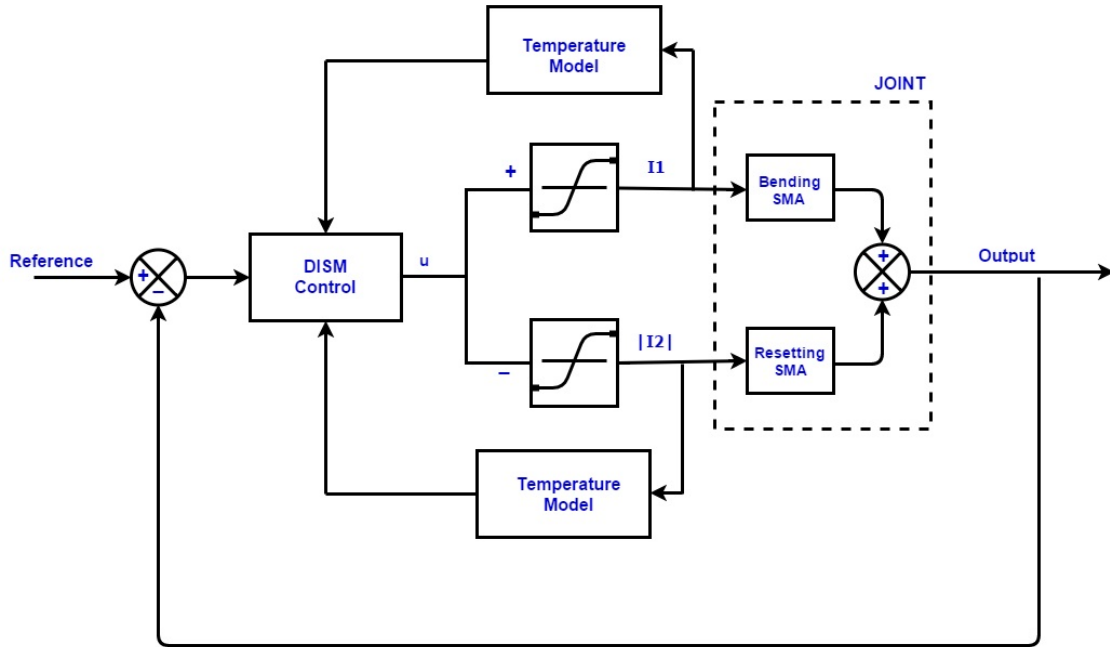
Figure 22: Block diargram of control strategy with temperature threshold

Featherstone et al worked on temperature estimation of SMA actuator based on measured resistance [54]. The resistance can be measured by measuring the voltage drop across the SMA actuator while the applied current is known and constant. For heating cycle, resistance plot against temperature change is shown in Fig. 4. The drawback of this method is that it is not accurate enough for cooling cycle. For cooling cycle no current should be provided to the system. To resolve this issue, a few milliamps of current was given and made sure that it shouldn't cause any change in temperature of the actuator. Results shows that resistance also have hysteresis nature related to temperature as shown in Fig. 23. Moreover, in [55] authors discussed the effect of change in applied stress. Electric resistance of SMA change with change in applied stress as it represents the phase change. In current design, stress feed-back is not available for the joint. In such case, reliable resistance measurement is not possible. Hence, temperature estimation based on electric resistance of SMA actuator is
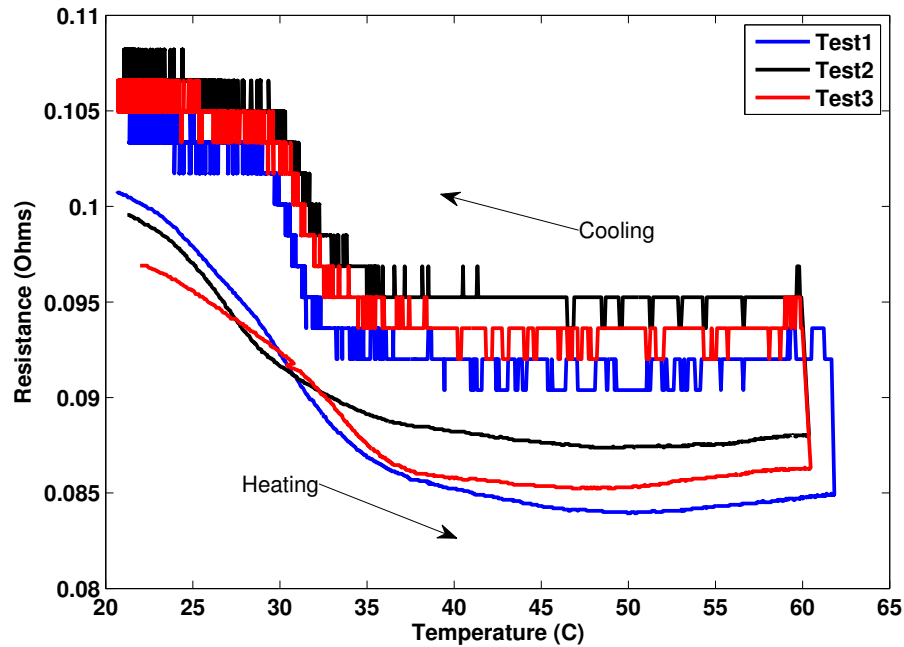
Figure 23: Hysteresis of resistance vs Temperature

not feasible.

- Other solution is to use the thermodynamics model based on Joule's heating which has been also used in the modeling of the SMA actuator. It can provide approximate temperature of the SMA with much less effort as compare to other two options mentioned above. Temperature model based on thermodynamics can be effected by change in environmental conditions. A reliable model can be obtain by characterizing the model parameters for specific environmental conditions like room temperature and heat convection coefficient. In the joint, position control of the SMA actuators is not based on temperature feedback. Hence, precise temperature estimation is not critical.

By comparing all the options explained above, the method of temperature modeling based on thermodynamics model is chosen. It is most appropriate for our application and feasible to obtain the optimized temperature model based on input current

46

provided by the controller. Details of temperature model are given in Section:2.3.1.1.

To define the threshold temperature value for actuators, we need to understand the effect of applied stresses over the SMA phase change and transformation temperatures. Stress effect is discussed in detail by Liang et al [32]and Brinson et al [33], [34]. Transformation temperatures changes with change in stress over the SMA and can be explained in term of Stress influence coefficient, C_A which is simply slope of Stress Vs Transformation temperature graph. In [33] Brinson et al defined the critical stress value based on C_A value is given below:

$$C_A(T - A_f) < \sigma < C_A(T - A_s) \tag{24}$$

where, T is the current temperature and A_s and A_f are austenite start and final temperatures, respectively. This expression describes the limitation of applied stress at specific temperature to complete the phase transformation. The temperature threshold value for our system is obtained as 26 °C. This temperature limit is found experimentally by considering the amount of stress applied by one wire on the other.

In order to find the C_A value for an SMA actuator an experiment was performed in which temperature was recorded during phase transformation by applying stress to the actuators in form of dead weight. C_A value for a specific SMA actuator was found as 0.15 $MPa/°C$ and the results are shown in Fig. 24.

4.6   Joint Control with Temperature Threshold

The temperature of the SMA actuators is estimated using Joule's law of thermodynamics. Results for position tracking in continuous motion are shown in Fig. 25. Continuous motion of the joint successfully achieved without the risk of damaging actuator due to the stresses at high temperature. Region of an in-active state is shown with double arrow. The in-active state of the controller is when it waits for the temperature of the respective actuator drops down to the temperature threshold value.
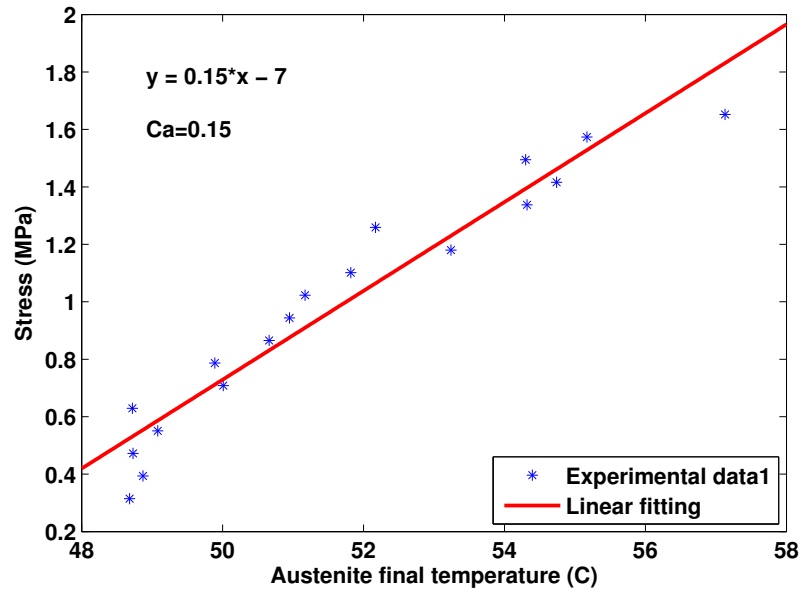
Figure 24: Stress influence coefficient, C_A value is obtained as slop of Austenite final temperature vs Stress plot

4.7 Position Control of Multiple Smart Joints using EMT sensors

In order to reach the target with complex passage, a tool with multi-DOF is required. Each joint can bend to approximately 60°. By connecting multiple joints in different combinations maneuverability of the tool can be increased. In this work, two joints are connected with rigid links in series with same direction of motion. In this way, tip can be bend up to 120°.

4.7.1 Position Control of Multiple Joints

Two smart joints are connected in series with rigid links as shown in Fig. 26. Bending direction of both joints is identical to increase the maneuverability of the tip of the tool.

Three EMT sensors are attached at the tip of the both joints and at the base, respectively. Sensors provides the absolute motion tracking hence, a sensor at the

base was needed to obtain the relative motion information. A code was written in MATLAB environment to communicate with NDI system and power supply.

The motion of two joints is controlled independent of each other. Multiple joint motion control is shown in Fig. 28 and the corresponding sensor data is shown in Fig. 27. The joint 1 and joint 2 were controlled independently with the precision of 0.0851 radians and 0.03665 radians of RMS error, respectively. In the region when catheter is resetting, relatively larger error can be seen which is due to in-active state of the controller controlled by the temperature threshold such as frame range for Joint 1 between 700 to 800.
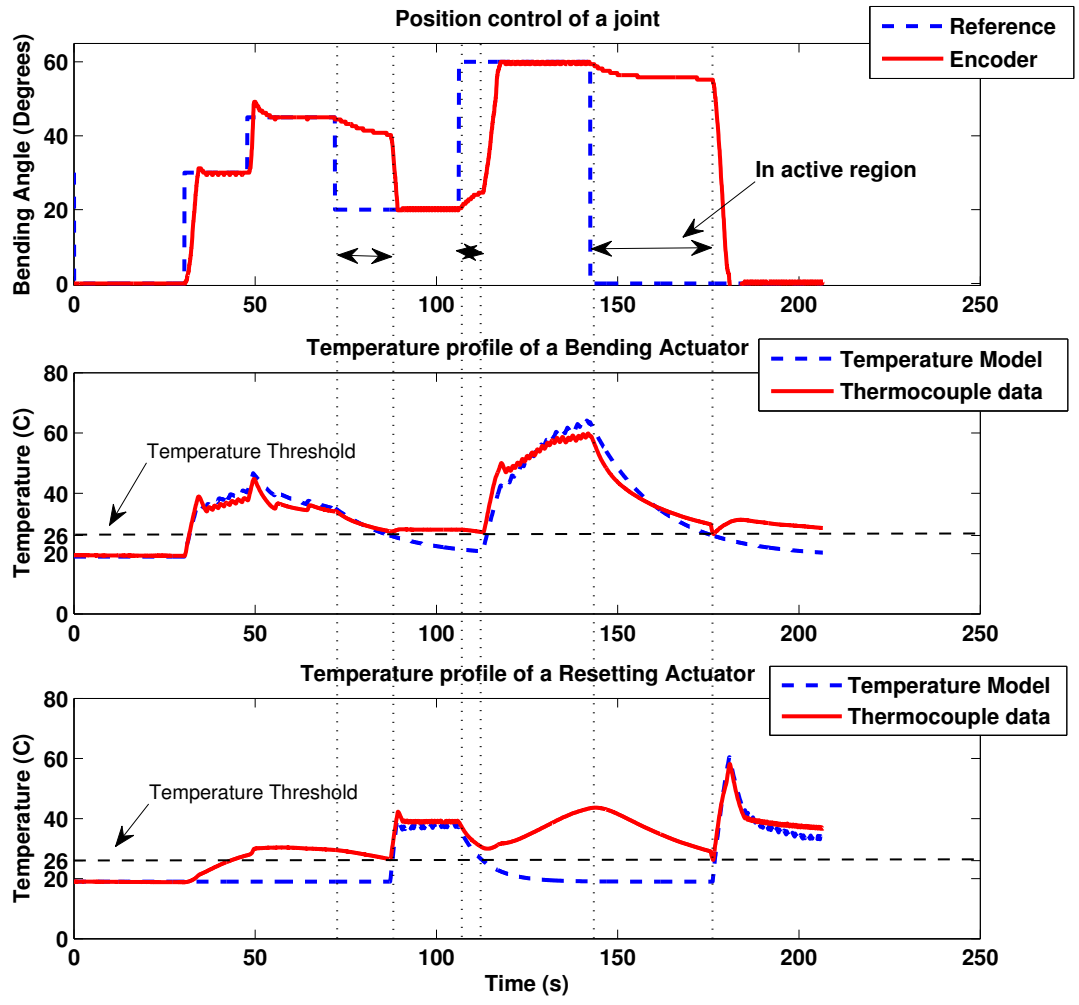
Figure 25: Continuous motion of the joint successfully achieved without the risk of damaging the actuator due to high stress at high temperature.
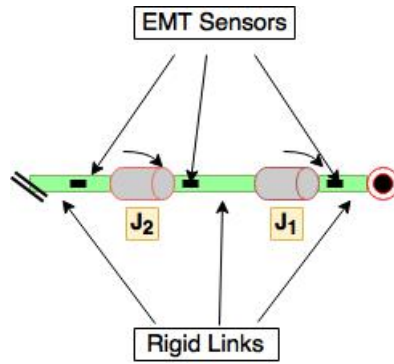
Figure 26: Multiple Joints connected with rigid links
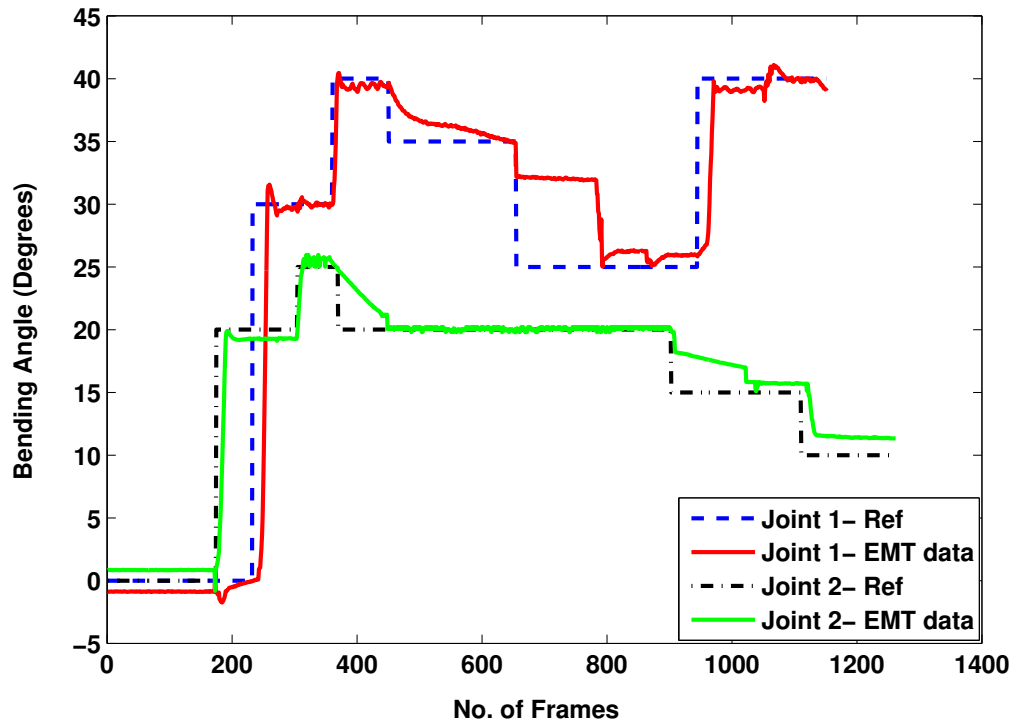

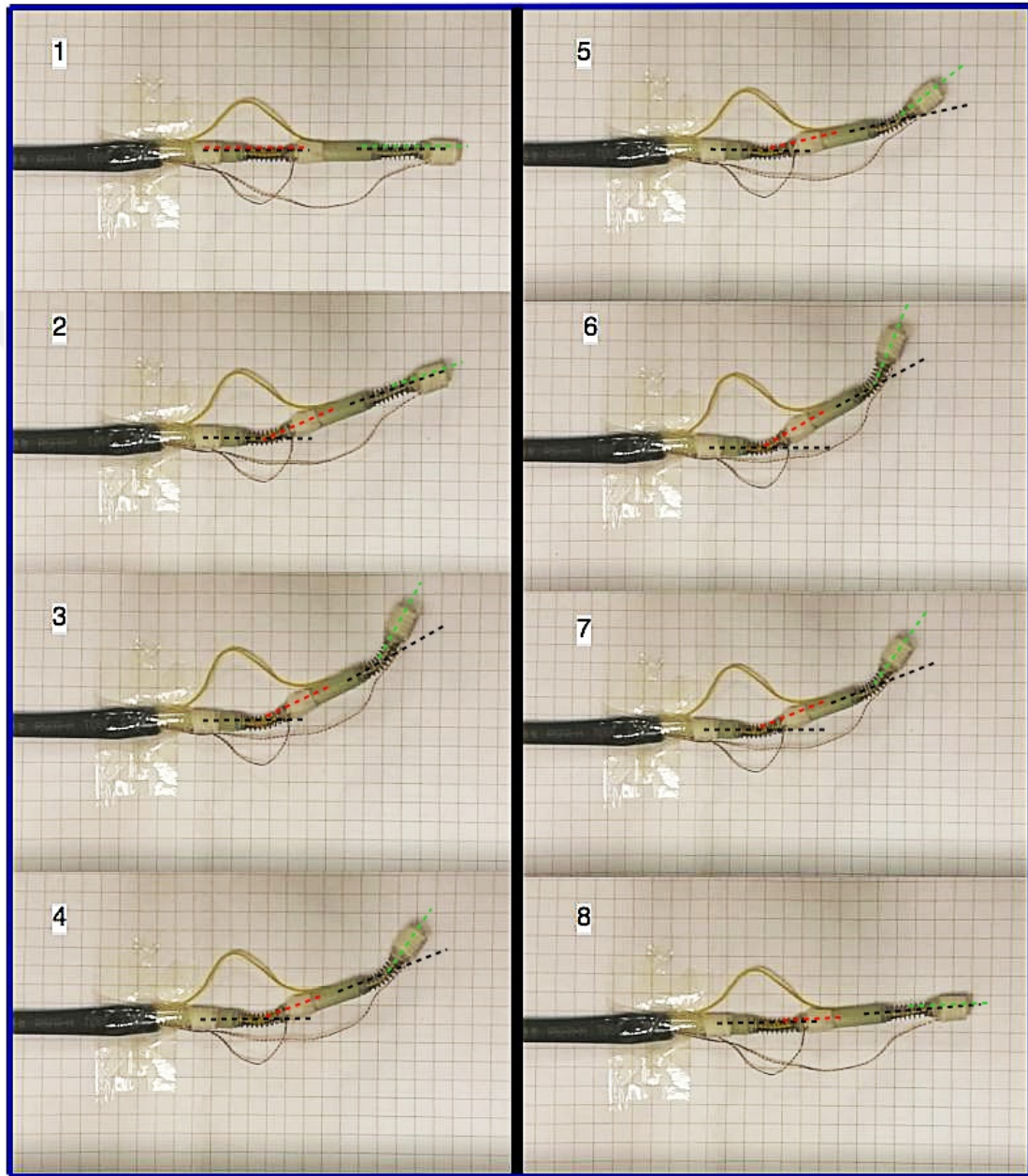**Figure 27:** Multiple joints EMT tracking results

Figure 28: Clips are taken from the video recorded during motion control of multiple joints. Motion was recorded by EMT sensors attached at the tips of both joints and at the base.

CHAPTER V

CONCLUSION

The aim of this thesis is to design a robust control scheme for motion control of a smart joint. Smart joints are designed on the base of Shape Memory Alloy (SMA) actuators. Two commercially available SMA wires of 0.6 mm diameter are heat treated to perform the bending and resetting action which provides the periodic motion to the joint. One SMA wire is heat treated for the bent shape to perform a bending action while the other wire is heat treated for the straight shape to perform a resetting action.

SMAs are modeled as nonlinear systems and the model parameters are prone to change with environmental changes and external disturbances. Model parameter uncertainties and sensitivity towards environmental changes can make the controller's job challenging. For model-based control schemes, a precise system model is required to ensure the better tracking performance. Hence, a control scheme was required which should be robust towards the model parameter uncertainties and external disturbances to eliminate the necessity of obtaining a precise system model.

The effort required to obtain the precise model of the SMA was reduced by making assumptions in the modeling. Stresses applied to the actuator during actuation were not estimated. Moreover, a nonlinear model was linearized to design the model based control scheme. A Sliding Mode Control (SMC) scheme was chosen due to its known properties of simple structure and robustness towards model parameter uncertainties. The SMC systems suffer from its chattering phenomenon which is undesirable specifically in medical applications where precise motion control is critical. Moreover, a continuous-time controller can make the low sampled data system unstable

about its steady-state. To solve this problem, a Discrete-time Integral Sliding Mode Control (DISMC) scheme is implemented to ensure the precise motion tracking. The model used to design the controller was roughly estimated and further simplified by linearization. Assumptions made in modeling were the main source of uncertainty in the system modeling. Hence, a Disturbance Observer (DOB) was integrated in the control scheme to estimate the disturbances and made the controller robust.

Working frequency of 0.1 Hz can be achieved if an improved cooling is provided to the joint during operation. Antagonistically arranged two SMA actuators have shown the effect on individual actuator's performance. Due to the fact that at high temperatures SMA exerts high forces, the active actuator may not perform equally well if the inactive actuator is at high temperature. Hence, the idealized frequency of 0.1 Hz was not achieved due to insufficient cooling. The bandwidth of smart joint mainly depends on the factor of cooling. For the provided cooling, continuous motion tracking with a minimum error of 0.0112 radians can be achieved with 0.04 Hz of response frequency. We suspect that an increase in RMS error at lower frequencies was due to heat transfer between SMA actuators. Temporary loss of performance happens when the inactive actuator is in austenite phase and exerts stresses higher than the critical stress value of the active actuator. While overheating of the actuator at stress higher than its critical value can effect the cyclic life of the joint. These results led us to add the temperature threshold control in the current control scheme which was solely based on the position feedback.

The temperature of SMA actuator is estimated using the Joule's law of thermodynamics. Temperature threshold controls the activation of position based control scheme. Controller waits until the temperature of respective actuator drops down to the temperature threshold value. By introducing the temperature threshold in DISMC system continuous motion of the joint was successfully achieved without the risk of damaging the actuator due to high stress at high temperature.

Finally, motion control of multiple joints was successfully performed. The joints were connected to each other with rigid links. In order to perform the tracking of the multiple joints, three ElectroMagnetic Tracking (EMT) sensors were attached at the tips of both joints and at the base, respectively, to provide position feed-back. EMT sensors provide the absolute motion tracking hence, a sensor at the base was needed to obtain the relative motion information. A code was written in the MATLAB environment to communicate with the NDI system and the power supply.

Bibliography

[1] I. Modlin, *Brief history of endoscopy (A).* Nexthealth, 2000.

[2] Y. Wang, D. R. Uecker, C. S. Jordan, J. W. Wright, K. P. Laby, and J. D. Wilson, "Method and apparatus for performing minimally invasive cardiac procedures," Jan. 5 1999. US Patent 5,855,583.

[3] P. A. Moskovitz, S. Boden, W. F. McKay, and J. Moctezuma, "Minimally invasive spinal surgical methods and instruments," Apr. 21 1998. US Patent 5,741,261.

[4] H. H. Ramadan and A. M. Terrell, "Balloon catheter sinuplasty and adenoidectomy in children with chronic rhinosinusitis," *Annals of Otology, Rhinology & Laryngology*, vol. 119, no. 9, p. 578, 2010.

[5] M. Jacobs, J. Verdeja, and H. Goldstein, "Minimally invasive colon resection (laparoscopic colectomy).," *Surgical Laparoscopy Endoscopy & Percutaneous Techniques*, vol. 1, no. 3, pp. 144–150, 1991.

[6] R. L. Weiss, C. A. Church, F. A. Kuhn, H. L. Levine, M. J. Sillers, and W. C. Vaughan, "Long-term outcome analysis of balloon catheter sinusotomy: two-year follow-up," *Otolaryngology-Head and Neck Surgery*, vol. 139, no. 3, pp. S38–S46, 2008.

[7] J. J. Regan, H. Yuan, and P. C. McAfee, "Laparoscopic fusion of the lumbar spine: minimally invasive spine surgery: a prospective multicenter study evaluating open and laparoscopic lumbar fusion," *Spine*, vol. 24, no. 4, pp. 402–411, 1999.

[8] L. H. Cohn, D. H. Adams, G. S. Couper, D. P. Bichell, D. M. Rosborough, S. P. Sears, and S. F. Aranki, "Minimally invasive cardiac valve surgery improves patient satisfaction while reducing costs of cardiac valve replacement and repair.," *Annals of surgery*, vol. 226, no. 4, p. 421, 1997.

[9] A. R. Abreu, M. A. Campos, and B. P. Krieger, "Pulmonary artery rupture induced by a pulmonary artery catheter: a case report and review of the literature," *Journal of Intensive Care Medicine*, vol. 19, no. 5, pp. 291–296, 2004.

[10] T. W. Duerig, K. Melton, and D. Stöckel, *Engineering aspects of shape memory alloys.* Butterworth-Heinemann, 2013.

[11] J. Ryhänen, M. Kallioinen, J. Tuukkanen, J. Junila, E. Niemelä, P. Sandvik, and W. Serlo, "In vivo biocompatibility evaluation of nickel-titanium shape memory metal alloy: Muscle and perineural tissue responses and encapsule membrane thickness," *Journal of biomedical materials research*, vol. 41, no. 3, pp. 481–488, 1998.

[12] T. Duerig, A. Pelton, and D. Stockel, "The use of superelasticity in medicine," *Metall-Heidelberg*, vol. 50, no. 9, pp. 569–574, 1996.

[13] J. D. W. Madden, N. A. Vandesteeg, P. A. Anquetil, P. G. A. Madden, A. Takshi, R. Z. Pytel, S. R. Lafontaine, P. A. Wieringa, and I. W. Hunter, "Artificial muscle technology: physical principles and naval prospects," *IEEE Journal of Oceanic Engineering*, vol. 29, pp. 706–728, July 2004.

[14] F. Migliavacca, L. Petrini, P. Massarotti, S. Schievano, F. Auricchio, and G. Dubini, "Stainless and shape memory alloy coronary stents: a computational study on the interaction with the vascular wall," *Biomechanics and modeling in mechanobiology*, vol. 2, no. 4, pp. 205–217, 2004.

[15] Y. Haga, Y. Tanahashi, and M. Esashi, "Small diameter active catheter using shape memory alloy," in *Micro Electro Mechanical Systems, 1998. MEMS 98. Proceedings., The Eleventh Annual International Workshop on*, pp. 419–424, IEEE, 1998.

[16] J. Swensen, M. Lin, A. Okamura, and N. Cowan, "Torsional dynamics of steerable needles: Modeling and fluoroscopic guidance," *Biomedical Engineering, IEEE Transactions on*, vol. 61, pp. 2707–2717, Nov 2014.

[17] M. Ho and J. P. Desai, "Characterization of antagonistic sma spring actuators for use in a mri-compatible intracranial robot," in *ASME 2012 5th Annual Dynamic Systems and Control Conference joint with the JSME 2012 11th Motion and Vibration Conference*, pp. 481–485, American Society of Mechanical Engineers, 2012.

[18] J. Pestana, R. Bombín, and E. García Armada, "Characterization of magnetic shape memory alloys (msma) oriented to periodic actuation," 2010.

[19] M. H. Elahinia, H. Ashrafiuon, M. Ahmadian, and H. Tan, "A temperature-based controller for a shape memory alloy actuator," *ASME. J. Vib. Acoust*, pp. 285–291, 2005.

[20] S.-H. Liu, T.-S. Huang, and J.-Y. Yen, "Tracking control of shape-memory-alloy actuators based on self-sensing feedback and inverse hysteresis compensation," *Sensors*, vol. 10, no. 1, p. 112, 2010.

[21] J. Pons, D. Reynaerts, J. Peirs, R. Ceres, and H. VanBrusse, "Comparison of different control approaches to drive sma actuators," in *Advanced Robotics, 1997. ICAR'97. Proceedings., 8th International Conference on*, pp. 819–824, IEEE, 1997.

[22] J. Jayender, R. V. Patel, S. Nikumb, and M. Ostojic, "Modeling and control of shape memory alloy actuators," *IEEE Transactions on Control Systems Technology*, vol. 16, pp. 279–287, March 2008.

[23] A. M. Franz, T. Haidegger, W. Birkfellner, K. Cleary, T. M. Peters, and L. Maier-Hein, "Electromagnetic tracking in medicine; a review of technology, validation, and applications," *IEEE Transactions on Medical Imaging*, vol. 33, pp. 1702–1725, Aug 2014.

[24] E. Ayvali, *Design, Development, and Evaluation of a Discretely Actuated Steerable Cannula.* PhD thesis, University of Maryland, College Park, 2014.

[25] D. C. Lagoudas, C. Li, D. A. Miller, and L. Rong, "Thermomechanical transformation fatigue of sma actuators," in *SPIE's 7th Annual International Symposium on Smart Structures and Materials*, pp. 420–429, International Society for Optics and Photonics, 2000.

[26] R. Abeyaratne, K. Sang-Joo, and J. K. Knowles, "A one-dimensional continuum model for shape-memory alloys," *International journal of solids and structures*, vol. 31, no. 16, pp. 2229–2249, 1994.

[27] S. Marfia, "Micro–macro analysis of shape memory alloy composites," *International Journal of Solids and Structures*, vol. 42, no. 13, pp. 3677–3699, 2005.

[28] F. Falk, "One-dimensional model of shape memory alloys," *Archives of Mechanics*, vol. 35, no. 1, pp. 63–84, 1983.

[29] F. Falk and P. Konopka, "Three-dimensional landau theory describing the martensitic phase transformation of shape-memory alloys," *Journal of Physics: Condensed Matter*, vol. 2, no. 1, p. 61, 1990.

[30] Y. Huo, "A mathematical model for the hysteresis in shape memory alloys," *Continuum Mechanics and Thermodynamics*, vol. 1, no. 4, pp. 283–303, 1989.

[31] K. Tanaka, "A thermomechanical sketch of shape memory effect: one-dimensional tensile behavior," *Materials Science Research International*, vol. 18, no. 251, 1985.

[32] C. Liang and C. A. Rogers, "One-dimensional thermomechanical constitutive relations for shape memory materials," *Journal of intelligent material systems and structures*, vol. 1, no. 2, pp. 207–234, 1990.

[33] L. Brinson, "One-dimensional constitutive behavior of shape memory alloys: Thermomechanical derivation with non-constant material functions and redefined martensite internal variable," vol. 4, no. 2, pp. 229–242, 1993.

[34] L. C. Brinson and M. S. Huang, "Simplifications and comparisons of shape memory alloy constitutive models," vol. 7, no. 1, pp. 108–114, 1996.

[35] H. Sayyaadi, M. R. Zakerzadeh, and H. Salehi, "A comparative analysis of some one-dimensional shape memory alloy constitutive models based on experimental tests," *Scientia Iranica*, vol. 19, no. 2, pp. 249–257, 2012.

[36] J.-H. Chung, J.-S. Heo, and J.-J. Lee, "Implementation strategy for the dual transformation region in the brinson sma constitutive model," *Smart Materials and Structures*, vol. 16, no. 1, p. N1, 2006.

[37] E. Ayvali and J. Desai, "Towards a discretely actuated steerable cannula," in *Robotics and Automation (ICRA), 2012 IEEE International Conference on*, pp. 1614–1619, May 2012.

[38] J. Carvajal, G. Chen, and H. Ogmen, "Fuzzy pid controller: Design, performance evaluation, and stability analysis," *Information Sciences*, vol. 123, no. 3, pp. 249–270, 2000.

[39] W.-D. Chang, R.-C. Hwang, and J.-G. Hsieh, "A self-tuning pid control for a class of nonlinear systems based on the lyapunov approach," *Journal of Process Control*, vol. 12, no. 2, pp. 233–242, 2002.

[40] G. Song, V. Chaudhry, and C. Batur, "Precision tracking control of shape memory alloy actuators using neural networks and a sliding-mode based robust controller," *Smart materials and structures*, vol. 12, no. 2, p. 223, 2003.

[41] J. C. Hannen, J. H. Crews, and G. D. Buckner, "Indirect intelligent sliding mode control of a shape memory alloy actuated flexible beam using hysteretic recurrent neural networks," *Smart Materials and Structures*, vol. 21, no. 8, p. 085015, 2012.

[42] D. Grant and V. Hayward, "Variable structure control of shape memory alloy actuators," *IEEE Control Systems*, vol. 17, no. 3, pp. 80–88, 1997.

[43] M. H. Elahinia and H. Ashrafiuon, "Nonlinear control of a shape memory alloy actuated manipulator," *Journal of vibration and acoustics*, vol. 124, no. 4, pp. 566–575, 2002.

[44] D. Zhang and S. Panda, "Chattering-free and fast-response sliding mode controller," *IEE Proceedings-Control Theory and Applications*, vol. 146, no. 2, pp. 171–177, 1999.

[45] G. Bartolini, A. Ferrara, E. Usai, and V. I. Utkin, "On multi-input chattering-free second-order sliding mode control," *IEEE transactions on automatic control*, vol. 45, no. 9, pp. 1711–1717, 2000.

[46] M. Roopaei and M. Z. Jahromi, "Chattering-free fuzzy sliding mode control in mimo uncertain systems," *Nonlinear Analysis: Theory, Methods & Applications*, vol. 71, no. 10, pp. 4430–4437, 2009.

[47] K. Furuta, "Sliding mode control of a discrete system," *Systems & Control Letters*, vol. 14, no. 2, pp. 145–152, 1990.

[48] G. Golo and Č. Milosavljević, "Robust discrete-time chattering free sliding mode control," *Systems & Control Letters*, vol. 41, no. 1, pp. 19–28, 2000.

[49] K. Abidi, J.-X. Xu, and Y. Xinghuo, "On the discrete-time integral sliding-mode control," *Automatic Control, IEEE Transactions on*, vol. 52, pp. 709–715, April 2007.

[50] M. C. de Oliveira, J. Bernussou, and J. C. Geromel, "A new discrete-time robust stability condition," *Systems & control letters*, vol. 37, no. 4, pp. 261–265, 1999.

[51] W. Gao, Y. Wang, and A. Homaifa, "Discrete-time variable structure control systems," *IEEE transactions on Industrial Electronics*, vol. 42, no. 2, pp. 117–122, 1995.

[52] A. Bartoszewicz, "Discrete-time quasi-sliding-mode control strategies," *IEEE Transactions on Industrial Electronics*, vol. 45, no. 4, pp. 633–637, 1998.

[53] K. Abidi and J.-X. Xu, *Advanced Discrete-Time Control.* Springer, 2015.

[54] R. Featherstone and Y. H. Teh, "Improving the speed of shape memory alloy actuators by faster electrical heating," in *Proceedings of the Ninth International Symposium on Experimental Robotics*, 2004.

[55] V. Novák, P. Šittner, G. Dayananda, F. Braz-Fernandes, and K. Mahesh, "Electric resistance variation of niti shape memory alloy wires in thermomechanical tests: Experiments and simulation," *Materials Science and Engineering: A*, vol. 481, pp. 127–133, 2008.

VITA

Ms. Saher Jabeen completed her bachelor's studies in the field of Mechatronics Engineering from Air University, Islamabad, Pakistan in September 2012. In 2014, she joined Ozyegin University with OzU Robotics Lab and started her MS degree in Mechanical engineering under the supervision of Assistant Professor Dr. Ozkan Bebek and Associate Professor Guney Guven Yapici. Her major research interest is Modeling and Control Systems in the field of Robotics.